Proceedings of the ASME 2024
International Design Engineering Technical Conferences and
Computers and Information in Engineering Conference
IDETC-CIE2024
August 25-28, 2024, Washington, DC

DETC2024-146374

KNOWLEDGE EXTRACTION IN ADDITIVE MANUFACTURING: A FORMAL CONCEPT ANALYSIS APPROACH

Yande Ndiaye[1,2,*], Mario Lezoche[1], Herve Panetto[1], Yan Lu[2], Zhuo Yang[2]

[1]Université de Lorraine, CNRS, CRAN, Nancy, France
[2]National Institute of Standards and Technology (NIST), Gaithersburg, MD, USA

ABSTRACT

In Additive Manufacturing (AM), it is still a major challenge to manage part quality, which is heavily influenced by feedstock materials, process settings, and in-process control. Deviations in these factors can lead to defects in the final product, particularly in Laser-Powder Bed Fusion (L-PBF), an AM process that builds parts with high precision but is too complex to control. On that account, in-situ monitoring becomes crucial for evaluating and ensuring process stability during L-PBF builds. By analyzing in-situ data, AM operators can detect process deviations and pause or stop a build as needed. Continuously monitoring in-situ data allows for immediate adjustments of process settings and avoids potential defects in the final part. However, the extensive amount of high dimensional data generated from advanced sensing technologies holds their benefit for anomaly detection and process control. The abundance and complexity of AM process monitoring data require a systematic approach to extract valuable insights and translate them into actionable knowledge. While machine learning-based techniques are nowadays essential for establishing AM process-structure-property relationships, they lack interpretability for quick actions from AM operators. In this context, we introduce a new methodology based on Formal Concept Analysis (FCA) to extract knowledge from AM multi-modal data as a set of association rules that could be used as a knowledge base to guide decisions and provide guidelines for AM operators. Specifically, for L-PBF, melt pool features are first extracted from in-situ melt pool images, and clustered into discrete categories through Machine Learning (ML) techniques. After that, FCA is allied and demonstrated to discover association rules revealing the intricate relationships between ranges of values of these features and process deviations. The final set of rules is analyzed and presented for users to adopt in monitoring their L-PBF AM processes.

*Corresponding author: ndeye.ndiaye@nist.gov, ndeye.ndiaye@telecomnancy.net

Documentation for `asmeconf.cls`: Version 1.36, June 20, 2024.

Keywords: Additive Manufacturing, Laser-Powder Bed Fusion, Data-driven, Data mining, Formal Concept Analysis, Knowledge extraction, Knowledge formalization

1. INTRODUCTION

In Additive Manufacturing (AM), optimizing and controlling manufacturing processes for part quality enhancement is paramount. The quality of an AM part is significantly impacted by factors such as the material used, process parameters, and the performance of the machine [1]. Alterations in actual material, process parameters, and machine settings could introduce deviations in the printing process leading to potential defects in the final part. Laser-Powder Bed Fusion (L-PBF) is one of the most commonly used AM techniques with which parts are created by successively melting materials layer by layer, following the instructions based on a 3D model [2]. Given the complexity of the processes and the intricate interplay of material characteristics, machine conditions, process settings, and control, a comprehensive understanding of the physics governing these interactions remains elusive. Nowadays, high-speed imaging sensors play a key role in monitoring and controlling metal-based AM processes, especially L-PBF. In-situ measurement, particularly melt pool monitoring, is widely used to observe the thermal conditions of the process and predict part quality in metal AM processes [3]. Sensors, co-axial or off-axis, generate high-resolution images of the melt pool and its surrounding areas, providing critical data that can be analyzed for real-time monitoring and decision-making. Nowadays, Artificial Intelligence (AI) models have emerged as pivotal tools, capable of quantifying process characteristics in real-time, detecting flaws, and predicting final part quality [4]. These models cluster or classify multi-modal data from various in-situ sensors to enhance process understanding and improve in-process decision-making and quality control. A considerable number of these models employ Deep Learning (DL), Supervised and Unsupervised Machine Learning (ML) to extract features from AM in-situ data for a variety of purposes, including process

monitoring, anomaly detection, and defect prediction [5]. As an example, Yeung et al. [6] designed a data-driven approach to model the impact of nearby laser scan positions on the properties of the melt pool in the L-PBF AM process. Their methodology based on the Neighboring-Effect Modeling method allows adjustment of the laser power based on the model's predictions to achieve a more uniform melt pool size but also minimize manufacturing defects in the final parts. Scime et al.[7] developed an algorithm for anomaly detection for powder bed monitoring that can automatically identify and categorize defects in an L-PBF machine with the use of clustering. Their approach was successfully applied to analyze numerous builds and provided valuable insights into build failure and to identify regions with potential defects in final parts. Kim et al. [8] used DL techniques such as Convolutional Neural Networks (CNNs) in a self-supervised learning context to predict melt pool orientation in the part based on laser scan strategy. Their methodology demonstrated the potential of DL for real-time process control and part quality prediction in LPBF, highlighting the significance of DL models to ensure optimal print quality.

Despite the efficiency of the AI approaches, there is still uncertainty about which variables from the multi-modal data are the key indicators for AM process stability and how they influence the process stability features, for example, melt pool size, shapes, and orientation [9]. With the aim of understanding the dependencies and correlations among multi-modal variables, this work proposes a new methodology based on Formal Concept Analysis (FCA), a data mining technique based on mathematical principles to clarify the relationships in AM multi-modal data and uncover the correlations between variables under normal operation.

This study uses in-situ high-sampling co-axial images to drive melt pool features such as size, width, length, shape, and intensities. These features are then clustered into categories through ML techniques. Finally, FCA is employed to discover association rules that reveal the intricate relationships between ranges of values of these features. In addition to the traditional FCA approach, our methodology incorporates the lift and conviction associations metrics to assess the strength and relevance of the associations between item sets in the rules to provide a more nuanced understanding of the relationships within the data. We also implement a refinement that fine-tunes the rules and enhances their clarity and applicability. With the developed methodology, our objective is to illustrate the potential of FCA to explore the associations between various features and their respective impacts on process stability. The final set of rules could be then used as a knowledge base to guide decision-making during a build process. Rule violations indicate process anomalies and the exact rules broken suggest the causes of the faults.

In summary, the key contributions of our work are as follows:

- Proposition of a new methodology based on Formal Concept Analysis (FCA) to analyze multi-modal data in Additive Manufacturing (AM) and extract knowledge.
- Integration of the lift and conviction metrics with FCA to enhance the understanding of relationships within the data.
- Provide a refined set of association rules to guide decision-making and identify process anomalies in AM.

This paper is divided into 4 sections. Chapter 2 describes the FCA-based methodology for knowledge extraction from AM data. In Chapter 3, we present the application of the methodology to a use case of a co-axial melt pool imaging system. Section 4 presents the result of the use case application. The results are discussed in Chapter 5, where the limitations and the future work are also presented. Finally, Section 6 summarizes the paper.

2. RESEARCH METHODOLOGY

This section presents a generalized methodology to extract knowledge from AM multi-modal data. The workflow; which consists of several steps, is presented with a description of the main concepts and approaches for better clarification and repeatability. The three principal stages of the methodology encompass multiple tasks, which are directed by a systematic approach that serves as a road map, as illustrated in Figure 1.

2.1 Data Preparation

Data preparation, the first step of the methodology, aims to optimize the efficiency of data analysis by ensuring high-quality data. This stage involves extracting the most pertinent information from large datasets, converting and reducing the data into a suitable format for mining, and finally rendering the dataset more manageable for analysis. In Data preparation, the raw data is collected from various sensors and optimal measurement instruments that record particularities happening during the AM process. Various types of data, including images, numerical data, and videos, could be gathered. After acquiring the data, we progress to the Data registration. This step is crucial as the raw data, collected from different measurement tools and sensors at various stages of the AM process, initially exist in disparate coordinate systems. By transforming this data into a single coordinate system, meaningful connections between different parameters can be established. To achieve this goal, Data fusion techniques can be employed. For example, Point-Based Registration can be used on images data to identify corresponding points in different datasets and estimate the transformation required for alignment [10]. This enables the integration of multiple datasets into a multi-modal dataset. The registered data can present noise, missing values, and irregularities. Therefore, the next step consists of cleaning it to eliminate any inconsistencies using Data pre-processing techniques [11]. Once the raw data is processed, we proceed to Features extraction aiming to extract relevant information and create a more robust dataset. This robust dataset is not only cleaned and organized but also enriched with key features that enhance the accuracy and reliability of further analyses. AI approaches could be used to extract relevant features of the specific task from the multi-modality data by reducing its dimension [12]. Finally, we progress to Data clustering where groups of data are created for the use of FCA, whose fundamental approach is limited to discrete data. Techniques from Unsupervised ML, such as clustering, can be used to discretize the data [13]. Especially, in the AM domain which frequently handles numerical

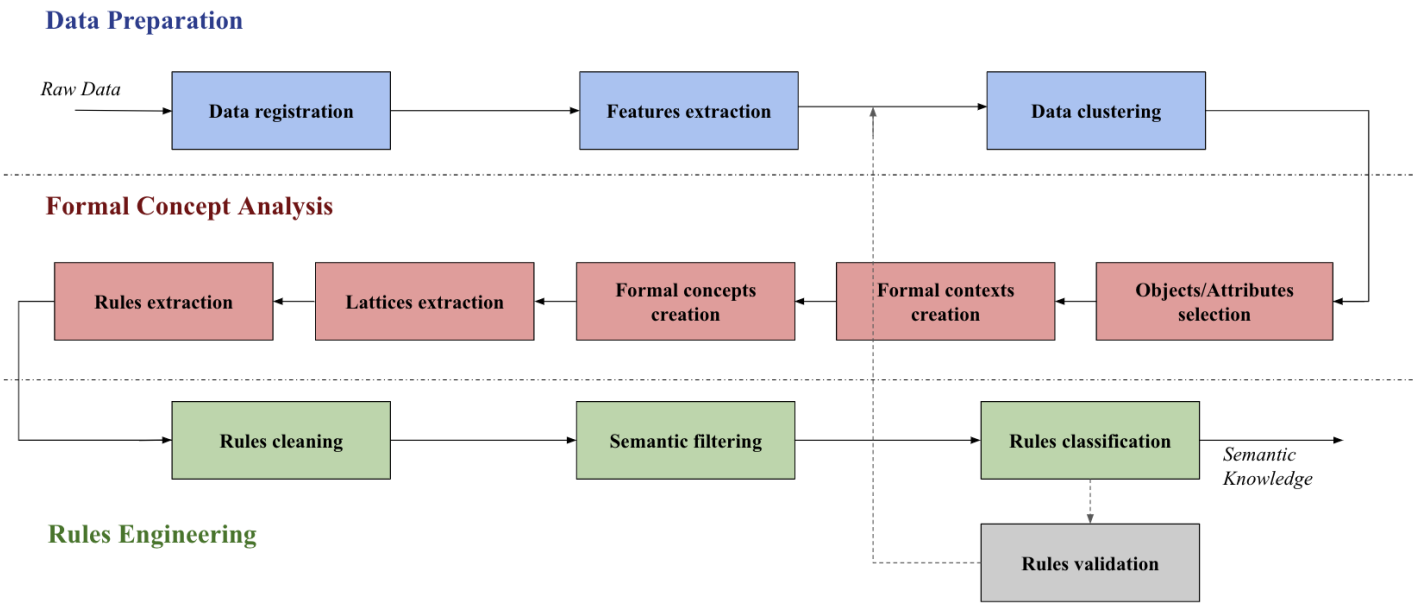

FIGURE 1: Workflow methodology

data, data clustering techniques, such as K-means [14] or hierarchical clustering [15], could help to group continuous values into distinct clusters. Each cluster can then be assigned a discrete label, making the data appropriate for FCA. Once the data is in a suitable format, we move on to the second major step of the methodology, which involves analyzing the data using FCA.

2.2 Formal Concept Analysis

Formal Concept Analysis (FCA) is a data mining technique that extracts relationships from a dataset containing *objects* and their characterizing *attributes*. FCA was introduced by Ganter et al. [16] as a mathematical framework based on the lattice theory. FCA is used in data analysis to identify and group similarities among data sets, forming conceptual hierarchies known as *concept lattices*. The *lattice* is employed to uncover and visualize the inherent structure within data by illustrating the relationships between *objects* and their *attributes* [17]. FCA has been widely used and has proved its efficiency across various disciplines such as biology, text mining, information retrieval, social networking, and software engineering for knowledge discovery [18]. Specifically, FCA is widely applied in biology to assist in the extraction of relevant information through the analysis of genetic material. For example, Ferré et al. [19], employed FCA to examine and understand the patterns of gene expression throughout various phases of bacterial development. Their method was effective in identifying crucial genes that play significant roles in bacterial development and basic cellular processes.

In FCA, the process starts by selecting sets of *objects* and *attributes* in a dataset to create the *formal context* which is a binary table that represents the relationships between selected *objects* and their *attributes*. Mathematically, a *formal context* is defined as a tuple $K(O, A, I)$, where:

- O is called the *objects*
- A is called the *attributes*
- $I \subseteq O \times A$ is a binary relation between O and A, called the incidence.

From each *formal context*, abstractions called *formal concepts* are derived to represent the intricate relationships between sets of *objects* and their common shared *attributes*. A *formal concept* is defined as a couple $C = (X, Y)$ such as $Y = X'$ [20]. X is called the *extent*, and Y the *intent*, of the concept C. Derivative operations are used to create the *formal concepts* from a *formal context*. The fundamental derivative operations are as follows. The object derivative X' takes a set of *objects* and maps it to all *attributes* shared by all those *objects*. Similarly, the derivative is applied on the *attributes*; the attribute derivative Y' takes a set of *attributes* and maps it to all *objects* that possess all these *attributes*. Therefore, the derivative of a set of *objects* X is the set of *attributes* in A shared by all the *objects* in X. Similarly, the derivative of a set of *attributes* Y, is the set of *objects* in O that jointly possess all the *attributes* of Y.

Mathematically, a *formal concept* of a *formal context* $K = (O, A, I)$ is a pair $C = (X, Y)$, in which:

1. $X \subseteq O$ and $Y \subseteq A$.
2. $\forall g \in O, \forall m \in A$:
   - $g \in X \iff (g, m) \in I, \forall m \in Y$.
   - $m \in Y \iff (g, m) \in I, \forall g \in X$.

The *formal concepts* derived from each *formal context*, are then ordered using mathematical principles to build a hierarchical structure called the *lattice*. In the *lattice*, *formal concepts* are organized as lower and upper *concepts* using an ordering relationship $\leq_K$.

Let's consider $C_1 = (X_1, Y_1)$ and $C_2 = (X_2, Y_2)$ two *formal concepts* of a *formal context* K. Within the *lattice* structure, we have the ordering relation;

$(X_1, Y_1) \leq_K (X_2, Y_2) \iff (X_1 \subseteq X_2$ (or equivalently $Y_2 \subseteq Y_1)$.

The partially ordered set $L_K = (C_K, \leq_K)$ is called the concept *lattice* of context K with C_K being the set of all *formal concepts*. Various algorithms can be found to extract *formal concepts* and build effectively the *lattice* in FCA. Notable algorithms in this field include Ganter's algorithm [21], the In-Close algorithm [22], and the Next-Closure algorithm originally presented by Wille [23] among others [18].

Finally, knowledge is extracted from the *lattice* as association rules using the inclusion relationships from upper and lower *formal concepts*. Numerous algorithms can be found for association rule mining, each one offering distinct methodologies and advantages depending on the structure and size of the data [24]. Distinguished algorithms in FCA include the Apriori algorithm by Agrawal et al. [25], the FP-Growth algorithm by Han et al. [26], and various incremental approaches [27].

2.3 Rules Engineering

After extracting the rules, we progress to the Rules engineering stage where the association rules are refined to eliminate any inconsistent or incoherent rules. Afterward, the rules are subject to semantic filtering based on selected features to retain the most relevant ones for the analysis task. Finally, the rules are classified based on the support and confidence which are common association rules metrics in FCA. Two other metrics are also incorporated in our methodology for further refining; the lift which evaluates the performance of an association rule, and the conviction which assesses the dependency of a rule's consequent on its antecedent.

Our methodology is generalizable to various AM data and processes. In the next Chapter, we demonstrate its practical applicability in the specific context of L-PBF AM. By analyzing co-axial melt pool images and extracting relationships from melt pool features and multi-modality data, our goal is to highlight the potential of our approach to provide valuable insights into the intricate dynamics of the AM process but also show the versatility and effectiveness of our methodology in addressing the complex challenges inherent in AM data analysis and knowledge extraction.

3. CASE STUDY

In this Chapter, we illustrate the applicability of the methodology by analyzing co-axial melt pool monitoring (MPM) images collected from the L-PBF AM process. The objective is to correlate melt pool features with the multi-modality data by uncovering discernible patterns and valuable insights from the MPM data.

3.1 The 3D Scan Strategy dataset

This work uses the 3D Scan Strategy dataset collected from the Additive Manufacturing Metrology Testbed (AMMT) at the National Institute of Standards and Technology (NIST). AMMT is a customized metrology system that offers flexible control and accurate measurement of the LPBF process [28]. A 3D build experiment was conducted by Lane et al. [29] resulting in 12 parts presenting the same dimensions; a roughly square structure of 10 mm by 10 mm by 5 mm. The build was made of powdered wrought nickel alloy 625 (IN625), each part consisted of several layers with a layer thickness of 3.2 mm. During the experiments, the laser power and scan speed varied between the 12 distinct parts. The height of each individual layer of the parts is 20 µm, and the diameter of the laser spot is 85 µm [29]. During the manufacturing process, in-situ measurements were collected by instruments on top of the AMMT. A co-axially aligned camera collected MPM images representing the melted area formed by the contact between the laser beam and the powder material. The camera maintained a steady focus on the melt pool, irrespective of the XY positioning of the galvo [28]. In the experimental setup, a unique approach to collect MPM data was adopted with co-axial MPM images collected for a single part for a specific layer. This specific pattern was repeated every 12 layers, aligning with the 12 different parts [29]. Figure 2 shows one of the created parts.

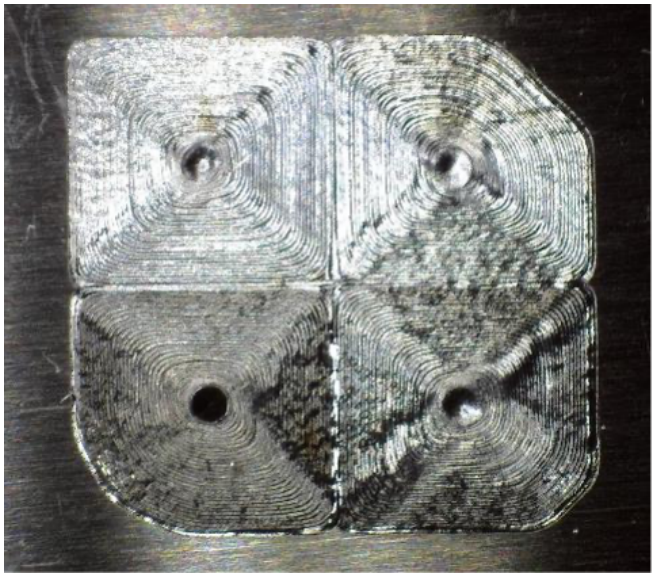

FIGURE 2: A 3D Scan Strategy part

The following sections detail the Data Preparation process, which focuses on formatting the data for mining purposes, followed by the application of the FCA procedure on melt pool features and multi-modal data, resulting in the generation of association rules that link variables magnitudes. Later, with the Rules Engineering step, we refine and present the final set of rules retained based on selected features of interest.

3.2 Data Preparation

3.2.1 Data collection. The data collected come from sensors and optical instruments on top of the AMMT machine. MPM images were collected from the co-axially aligned camera on top

of the AMMT. Our analysis focused on data collected for part 9 at layer 21, where each collected image represents a data point at a specific location in the part. Laser power and laser scan speed values at each location were gathered from AMMT sensors to create the dataset. For the analyzed layer, a total of 4958 MPM images were collected.

3.2.2 Data registration. The collected data were already registered. Point-Based Registration technique, using camera triggers as reference points to synchronize the MPM images was used for registration [29]. This method involves matching corresponding points in the images to calculate the transformation needed for alignment. By aligning the images to a common coordinate system, a coherent and integrated dataset was created, facilitating the analysis and interpretation of the melt pool dynamics in the L-PBF AM process. The collected images can display a melt pool and sometimes not. The images on the right in Figure 3 clearly show detectable melt pools for certain data points. The bright regions in these images indicate the melt pools, which vary by size, position, and intensity. Laser power and laser scan speed values for each MPM image were gathered from AMMT sensors to create the dataset.

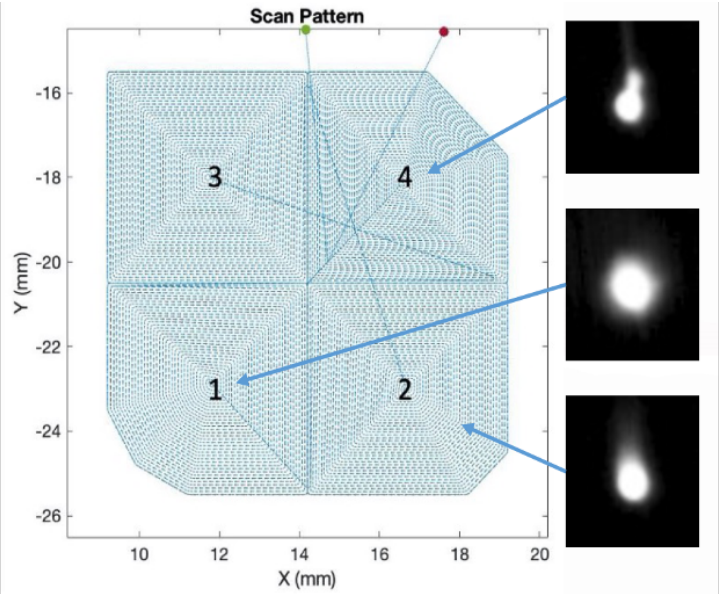

FIGURE 3: MPM images captured by the co-axially aligned camera for a 3D Scan Strategy part

3.2.3 Features extraction. Once acquiring the registered data, key features could be extracted. Image processing techniques, specifically edge detection and shape approximation, were used to extract features from the registered images [10]. In our use case, characteristics of the melt pool, including size, width, length, and ratio of the length to the width were extracted. These features were then organized into data tables for each set of images collected in the experiments for a specific layer. Each line in a data table describes an MPM image corresponding to a data point in the part. For layer 21 of part 9, a total of 4958 data entries were produced, corresponding to the 4958 MPM images gathered. For each data point, the corresponding melt pool information is extracted. Furthermore, process parameters such as laser power, laser scan speed, and scan pattern, related to each data point, are also included in the study. Among the collected co-axial images, some did not show any melt pool. Consequently, rows without melt pool information were removed from the data table, resulting in 4942 data points. Table 1 shows the process parameters and the melt pool features extracted. Figure 10 in Appendix A displays a portion of the table generated after features extraction.

3.2.4 Data clustering. After extracting relevant features from the images, we proceed to Data clustering, a key phase in the methodology because FCA needs discrete values to mine data. With Data clustering, we aim to transform numerical variables into FCA-compatible intervals. In this aim, Unsupervised ML techniques can be useful here, as they can handle the vast, unstructured AM data without relying on labeled data. Unsupervised ML was used in Data clustering to create distinct groups of data. For our use case, the K-means clustering algorithm was chosen to cluster the data, due to its simplicity and computational effectiveness. K-means is proven efficient in processing substantial data amounts and in creating non-overlapping clusters, suitable for varied data types and distributions [30]. We used the KMeans class from the sklearn.cluster in scikit-learn for Python, leveraging its user-friendly features for customized clustering. The optimal number of clusters for each parameter was determined using the silhouette method [31]. For each single variable of the dataset, the K-means algorithm from the Python library scikit-learn was applied across different cluster numbers, and silhouette scores were computed to assess cluster quality. By plotting these scores, the optimal number of clusters was identified at the highest point on the silhouette score curve, indicating the best data segregation. This helped in organizing continuous variables into discrete groups, facilitating the next research phase involving FCA. The process resulted in a data table saved as a CSV file, aiding in intricate rule extraction and analysis. Last column of Table 1 shows the optimum number of clusters obtained for each parameter.

Once the data was processed, we transformed our dataset into a binary format where each column of the table represented different clusters. For every row, a '1' was marked to indicate that the parameter value falls within the range of the corresponding cluster. Conversely, a '0' was used to denote no correlation, signifying that the parameter value does not belong to the particular cluster. Therefore, each data point's parameter value is linked to its corresponding cluster using these binary indicators, where '1' denotes inclusion in the cluster and '0' indicating exclusion. Figure 4 show parts of the CSV created for the Melt pool thermal analysis, where the columns represent the clusters variable and the lines represent the data points. This data structure enabled us to proceed with FCA, which is the next phase in our analysis.

3.3 Formal Concept Analysis

After preparing the data we had a suitable format for extracting association rules and applying FCA. ConExp (Concept Explorer), an open-source software for FCA was employed to this aim [32]. ConExp stands out for its user-friendly graphical interface, enabling easy visualization of formal concepts and

TABLE 1: Process parameters and melt pool features

Process input	Description	Value	Unit	Optimum number of clusters
Scan speed (v)	Laser scan speed	Nominal value: 800, varies	mm/s	8
Laser power (P)	Laser power	Nominal value: 195, varies	W	9
MPM features	**Description**	**Value**	**Unit**	**Optimum number of clusters**
x	Coordinate of the data point in x-axis position within the image coordinate system	Varies	mm	2
y	Coordinate of the data point in y-axis position within the image coordinate system	Varies	mm	2
Length	Melt pool length	Varies	mm	2
Width	Melt pool width	Varies	mm	3
Area	Surface of the melt pool	Varies	mm^2	3
Ratio	Ratio of the length to the width of the melt pool	Varies	-	2
Image intensity	Level of intensity for the entire MPM image	Varies	-	3
Melt pool intensity	Level of intensity of the melt pool	Varies	-	2

their relationships. This enhances data exploration by simplifying the understanding of complex concept networks. The tool is particularly adept at generating lattice structures crucial in FCA, offering a hierarchical view of concepts and their connections. The capabilities in ConExp extend beyond basic FCA operations by including association rule mining, and attribute exploration, allowing for complete analysis.

3.3.1 Objects-Attributes selection. In L-PBF AM process, melt pool plays a critical role and is closely monitored [33]. The melt pool is the small area where the laser beam causes the powder material to melt, resulting in a concentrated and liquefied area. This region is crucial since it represents the point at which the material undergoes a phase transition from a solid state to a liquid state, and then back to a solid state [34]. Melt pool geometry directly influences the stability of the process and the properties of the final material [35]. Studies show that the size and shape of the melt pool affect the microstructure and mechanical properties of AM-produced parts [35]. Indeed, inadequate melt pool formation can lead to porosity in parts, which is often caused by lack of fusion or trapped gas [36]. To improve the quality of AM parts, controlling the melt pool size and reducing its variations in the melt pool is up of importance. However, melt pool formation depends on various factors such as the energy density, which has been found to significantly impact melt pool size [35]. Thus, adjusting processing parameters such as laser power, and scanning speed could help monitor the melt pool. However, this approach has limitations, as melt pool size can still vary due to uncontrollable factors like part geometry or environmental conditions. This variability can lead to melt pool anomalies, which if not detected and corrected, can result in poor material properties or part failures [37].

To clarify how these process features affect the melt pool size, we proceeded to the Process dynamics and derived melt pool ratio analysis. Therefore, we selected process characteristics such as laser power and laser speed, and the melt pool ratio feature to investigate the correlation between these variables. The aim is to study how process parameters affect the melt pool ratio.

To analyze the thermal dynamics of the melt pool, we also studied the interdependence between clusters of melt pool size, melt pool intensity, and the entire image intensity. With this analysis, we aim to uncover how the melt pool sizes can be detected with the intensity of the image and the melt pool captured by the instruments on the AMMT.

From the CSV obtained after Data clustering, we generated two new CSV files with clusters for the chosen variables for each analysis task. The columns in the files contain the cluster names and reflect the attributes, while the rows represent the data points (MPM images) representing the objects. Each object is connected to the attributes using a binary connection, where a value of 1 indicates the association with the data point (and consequently the melt pool image). For each object, when the value of the feature or parameter belongs to the assigned cluster, it is denoted as '1'. If the parameter value for the current object is not part of the specified cluster, it is represented by the value '0.' After creating the CSV structures, the files needed to be processed to be uploaded in ConExp to visualize the two formal context tables.

3.3.2 Formal context creation. To effectively use ConExp, the data needs to be transformed from CSV to CEX format, which is necessary as ConExp exclusively supports this format. A CEX file offers a binary representation of the connections between objects and their attributes, leveraging an XML-like structure for hierarchical data representation. A Python script was created to convert the CSV files to CEX formats while maintaining the essential attributes of the data for FCA. The CEX files were formatted using XML and comprise a tag-value structure with root elements, an Attributes section, and an Objects section. The

	a0	a1	a2	iml0	iml1	iml2	mpml0	mpml1
p1	1	0	0	1	0	0	1	0
p2	1	0	0	1	0	0	1	0
p3	1	0	0	1	0	0	1	0
p4	1	0	0	1	0	0	1	0
p5	1	0	0	1	0	0	1	0
p6	1	0	0	1	0	0	1	0
p7	1	0	0	1	0	0	1	0
p8	1	0	0	1	0	0	1	0
p9	1	0	0	1	0	0	1	0
p10	1	0	0	1	0	0	1	0
p11	1	0	0	1	0	0	1	0
p12	1	0	0	1	0	0	0	1
p13	1	0	0	1	0	0	0	1
p14	1	0	0	1	0	0	1	0
p15	1	0	0	1	0	0	1	0
...	...	...	...	...	...	...	...	...
p3413	0	1	0	0	1	0	0	1
...	...	...	...	...	...	...	...	...
p4942	1	0	0	1	0	0	0	1

FIGURE 4: Part of the CSV file created after single-variable clustering for the Melt pool thermal analysis

root elements consist of tags for the conceptual system, version, and contexts. The Attributes section presents all attributes with distinct identifiers and names, while the Objects section lists all objects, each having a name and an intent tag that indicates their connection to attributes. Two CEX structures were created corresponding to the Process dynamics and derived melt pool ratio analysis and the Melt pool thermal analysis. The files were uploaded in ConExp resulting in the creation of a formal context table for each analysis task.

3.3.3 Formal concepts creation. Formal concepts were derived from each formal context table. Each formal concept is represented by a node with the set of objects representing individual data points and called the Extent whereas attributes indicate the clusters to which these data points could be assigned and called the Intent. From the formal contexts, 169 formal concepts were generated for the Process dynamics and derived Melt pool ratio analysis, while 43 were extracted for the Melt pool thermal analysis.

3.3.4 Lattice creation. After generating the formal concepts, the next objective is to construct the lattice. The Concept lattice helps to visualize the relationships between the formal Concepts by showing their organized structure. It is composed of nodes and edges, where each node represents a formal concept, denoting a distinct collection of objects and their common attributes. The edges in the lattice show the hierarchical relationship between the formal concepts. An edge connects two formal concepts when one is a sub-concept of the other, with no intermediate concepts between them. Nodes higher in the lattice are called the super-concepts, while lower nodes are sub-concepts. A Super-concept is a higher-level formal concept that includes a larger set of objects but fewer attributes. Each concept in the lattice is associated with an immediate super-concept, directly above it and linked by an edge. A Sub-concept is a lower-level concept containing a smaller set of objects with more attributes. The immediate Sub-concept of a concept is the node directly below it, connected by an edge.

Two lattices were created, each based on the formal context represented for each analysis task. Figure 11 in Appendix B, shows the lattice produced for the Melt pool thermal analysis. Each node represents a formal concept, labeled as (A, B), where A represents a group of objects and B represents a set of attributes. Every object in set A has all attributes in set B, and conversely. The diagram shows the basic intersection that includes only the top-level super-concepts and bottom-level sub-concepts for clarified representation.

3.3.5 Rules extraction. After creating the concept lattices in ConExp, the association rules were derived. In data mining, an association rule establish relationships between different items in a dataset. An association rule is typically represented as $A \rightarrow B$, in which A and B are subsets of items from a set of attributes. In FCA, such a rule is evaluated using the confidence and support metrics. The support measures the proportion of transactions containing A and B, while the confidence measures the proportion of transactions in the dataset containing B when A is present.

Many algorithms can be used to derive the association rules. ConExp makes use of the Duquenne-Guigues Basis and the Luxenburger Base to derive association rules. The Duquenne-Guigues Basis emphasizes strict implications, establishing clear connections in the data and providing a unique foundation for inferring additional implications [38]. The Luxenburger Base is designed to create approximation rules that capture significant patterns and probabilities using a wide range of connections that reflect real-world complexity [39]. The association rules feature in ConExp is used to derive association rules from any lattice. It helps ConExp explore the lattice and detect strong implications and approximation rules. The rules are given with unique support and confidence levels. An example of the FCA procedure for the Melt pool thermal analysis is depicted in Figure 5. For the Process dynamics and derived Melt pool aspect analysis, 270 association rules were extracted, while the Melt pool thermal analysis generated 51 association rules. Given the large number of rules extracted, we proceeded to Rules Engineering to refine and consolidate them for practical application, ensuring they provide meaningful and coherent insights for decision-making and analysis.

3.4 Rules Engineering

As seen with the two analysis tasks, deriving association rules from datasets can result in an extensive set of rules. Many of the extracted rules lack consistent and useful insights, showing contradictions or incoherence that go against the logic of the data. Thus, it is essential to refine these rules systematically to transform them into actionable insights for making informed

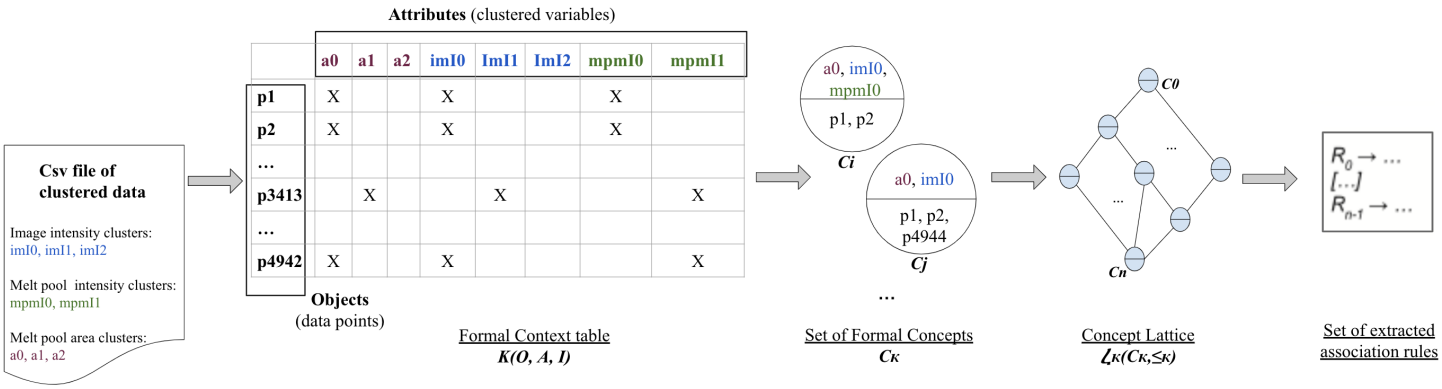

FIGURE 5: FCA procedure for the Melt pool thermal analysis

decisions and conducting meaningful analyses. To tackle this issue, we proceeded to the Rules cleaning step which consists in removing inconsistent and incoherent rules.

3.4.1 Incoherent rules. Among the set of association rules, we found what we have called Incoherent rules. These rules are characterized by their lack of logical consistency or practical applicability. As part of the refinement process, we address these issues by first removing any such rules that contain redundancies or contradictions. For example, a rule stating $Power1, Power2 \rightarrow Meltpoollength1$ is considered incoherent and thus discarded, as it defies logic for a single power value to be associated with both the Power1 and Power2 clusters simultaneously.

3.4.2 Inconsistent rules. We define an inconsistent rule $A \rightarrow B$, if $A = \emptyset$ or $B = \emptyset$. The absence of any specific antecedent suggests that for such a rule, B occurs with certainty but without any identifiable cause which suggests that a specific parameter will have a given value with an associated probability, irrespective of any circumstances. Such a rule lacks insightful information. Moreover, an association rule should ideally indicate that the presence of A raises the probability of B occurring. Therefore, any rule with this structure is eliminated from the set of association rules. Similarly, rules missing a consequent are also eliminated. A Python code was developed to remove incoherent and inconsistent rules, leading to the removal of 96 rules out of the total of 270 association rules for Process dynamics and derived melt pool ratio, while 12 rules were removed for the Melt pool thermal analysis.

3.4.3 Semantic filtering. Although prior Rules cleaning allowed to decrease the number of rules, not all of them remain of interest. With Semantic filtering, we concentrate on the qualitative rules that provide valuable insights to guarantee a final set of rules that are contextually pertinent to our analysis goals. In this aim, we refined the association rules by filtering the rules based on features of interest.

For the analysis of Process dynamics and derived melt pool ratio, we filtered the rules expressing melt pool ratio clusters based on laser power and laser speed clusters. This resulted in a total of 86 rules selected from the 174 rules obtained after rules cleaning.

The Melt Pool thermal analysis aims to study the relationships between image intensities, melt pool intensities, and melt pool areas. Studying the relationship between image intensity, melt pool intensity could help characterize the melt pool size and provide valuable information on the thermal dynamics. In this aim, we filtered the rules that express melt pool area clusters based on melt pool and image intensity clusters. Out of the 39 rules obtained after cleaning, 13 rules meet the given criteria.

3.4.4 Rules classification. With the set of association rules selected, we proceeded to analyze their strength and reliability, using traditional measures coming with FCA; the support and the confidence. The support is a fundamental metric in FCA. For a rule $A \rightarrow B$, it represents the probability of having A or B in the dataset. The confidence represents the probability of having B given A. For a rule $A \rightarrow B$ the support and confidence are defined as follows in Eq. (1) and Eq. (2).

$$Support(A \rightarrow B) = Probability(A \cup B) \quad \text{range} \in [0, 1] \tag{1}$$

$$Confidence(A \rightarrow B) = \frac{Support(A \rightarrow B)}{Support(A)} \quad \text{range} \in [0, 1] \tag{2}$$

Two other metrics were added to our methodology the lift and the conviction measures. These metrics were calculated and offered greater insights into the effectiveness and reliability of the association rules.

The lift metric indicates the rule's performance by demonstrating how often the antecedent and consequent occur together, more than would be expected if they were independent [40]. A lift value larger than 1 indicates a positive association between the antecedent and consequent of a rule. The conviction provides

the rule's predictive capacity by comparing the frequency of incorrect predictions to what would be expected if A and B were independent [41]. The higher the conviction value is, the more robust the rule is. The lift and conviction measures are added to our FCA-based methodology. For an association rule $A \Rightarrow B$, the value of these metrics is provided as follows in Eq. (3) and in Eq. (4).

$$Lift(A \rightarrow B) = \frac{Confidence(A \rightarrow B)}{Support(B)} \quad \text{range} \in [0, +\infty] \tag{3}$$

$$Conviction(A \rightarrow B) = \frac{1 - Support(B)}{1 - Confidence(A \rightarrow B)} \quad \text{range} \in [0, +\infty] \tag{4}$$

By including these two metrics in our methodology, we intend to strengthen the robustness of the association rules and find the strongest and most reliable ones. This technique allowed us to provide a fuller analysis, avoiding biases that may emerge from over-reliance on support and confidence metrics. Furthermore, our goal was to classify the rules to prioritize those crucial for informed decision-making in the AM domain. The rules were classified in Python using a combination of the mentioned metrics, prioritizing those that have higher confidence and conviction values to represent the strongest rules.

3.4.5 Rules validation. To assess the robustness, accuracy, and relevance of the refined rules, we conducted a validation phase. This procedure evaluated the coherence of the rules with the training layer; layer 21. Validation of the rules was also tested across different datasets to assess their general applicability beyond the specific conditions of the analyzed layer. For each rule, we calculated the real support and confidence and compared it with the rules' predicted confidence. Especially, we focused on layers 9, 33, and 69 from part 9. This step is crucial for verifying the integrity and consistency of our findings across varied data contexts. Moreover, this enables confident decision-making from the extracted rules.

Proceeding to the Rules Engineering steps allowed us to effectively decrease the quantity of association rules to a more manageable collection. In the next chapter, we will comprehensively examine some of the obtained rules, extract useful insights, and draw conclusions that could provide valuable insights for decision-making in the AM domain.

4. RESULTS

In this chapter, we present the results of the FCA-based methodology for the Process dynamics and derived melt pool ratio analysis and for the Melt pool thermal analysis. The retained association rules for each analysis task are presented and we try to interpret some of them to understand how melt pool features are influenced by the the laser scan speed and laser power, but also how these features are linked to the process signature of the build.

4.1 Data clustering

As seen in the previous Chapter, our process started with the collection of registered data from sensors and optical instruments on top of the AMMT machine. Then melt pool features were extracted from the registered MPM images to establish a dataset. The dataset contained details for each MPM image data point, including coordinates, laser power, scan speed, melt pool size, and different intensity values. We grouped values of single parameters using the K-Means ML model. The clusters yielded specific ranges for laser power, scan speed settings, and melt pool properties. Appendix C describes the result of Data clustering, for the set of parameters considered for both Melt pool analysis.

4.2 Final set of rules

The Melt pool thermal analysis aims to establish correlations between clusters representing melt pool and image intensities with melt pool area clusters. Therefore, after cleaning the initial set of 51 rules obtained using FCA, we semantically filtered the rules by focusing on those expressing melt pool area clusters based on melt pool intensity and image intensity clusters. Similarly, to analyze the effect of process dynamics on the melt pool areas, we filtered the rules obtained for the Process dynamics and derived melt pool ratio analysis, and retained the rules expressing melt pool area clusters based on laser power and laser speed clusters.

Table 2 displays the number of association rules generated at each stage of the Rules engineering process for each analysis task.

4.2.1 Process dynamics and derived melt pool ratio. The objective of studying Process dynamics and melt pool ratio is to establish relationships between clusters of laser power, laser speed, and melt pool ratio. Through our methodology, 86 rules that describe the melt pool ratio based on clusters of laser power and laser scan speed were retained. Given the large number of rules, we will only discuss the rules with the highest metric values. However, the final set of rules can be found in Appendix E for more details.

1. Rule: P0, v5 → r1, Support: 0.02%, Confidence: 100%, Lift: 4943, Conviction: 1e+10
   This rule suggests that the combination of the lowest laser power (P0) and high scan speed (v5) leads to a lower melt pool ratio (r1).

2. Rule: P1, v0 → r0, Support: 0.02%, Confidence: 100%, Lift: 4943, Conviction: 1e+10

3. Rule: P4, v0 → r0, Support: 0.02%, Confidence: 100%, Lift: 4943, Conviction: 1e+10
   Rule 2 and 3 state that a slightly higher laser power (P1 and P4) along with the lowest scan speed (v0) results in the smallest melt pool ratio (r0).

4. Rule: P6, v6 → r0, Support: 0.02%, Confidence: 100%, Lift: 4943, Conviction: 1e+10
   This rule, suggests that every time that laser power P6 and laser scan speed v6 are set, the melt pool ratio is observed to be in the range r0.

TABLE 2: Number of association rules retained after Rules engineering for each melt pool analysis tasks

Analysis task	Initial number of association rules	Number of association rules after cleaning	Number of association rules after filtering
Process dynamics and derived melt pool ratio	270	174	86
Melt pool thermal analysis	50	38	13

Rules 1, 2, 3, and 4 stand out with the highest lift values and among the rules with the highest confidence. These rules are among the rules with the lowest support values, indicating that while the occurrence of the antecedent of these rules increases the probability of having the consequent significantly, these conditions are relatively rare in the dataset. This could suggest that the scenarios captured by these rules are very specific and only occur under unique circumstances. Despite the rarity, these rules are very reliable. Indeed, the certainty of having the consequent given the antecedent is absolute, as seen by the highest confidence values of 100%.

With the highest support value, Rule 86: v6 $\rightarrow$ r0 is the most frequent occurrence in the dataset, appearing in 25.77% of all transactions. The rule indicates that when operating at laser speed in range v6, there is a 54% chance that the melt pool ratio will be within the range of r0. The lift value of 2.10 is the lowest from the entire set of rules. However, the positive value indicates that the probability of witnessing a melt pool ratio within the range r0 is 2.1 times greater when the laser scan speed falls within the range v6, as opposed to when it is outside this range. The conviction of this rule is one of the lowest with a value of 1.61 suggesting a modest dependence of the melt pool ratio r0 on the laser scan speed v6.

4.2.2 Melt pool thermal analysis. The Melt pool thermal analysis aims to extract relationships between clusters of melt pool area, melt pool intensity, and image intensity. The goal is to see how melt pool area can be determined based on image and melt pool intensity. The set of 13 association rules retained after the Rules Engineering process is provided in Appendix D.

Rule 1 stands out from the final set of rules with the highest confidence, lift, and conviction values. The rule suggests that when image intensity ranges from 18.40 to 29.82 and the melt pool intensity ranges from 177.25 to 204.09, the melt pool area is expected to range from 0.041152 mm^2 to 0.082432 mm^2 so the larger melt pool size. The 100% high confidence indicates that the combination of having image intensity in the range of imI2 and melt pool intensity in the range of cluster mpmI1 consistently leads to the larger melt pool area a2. However, the low support value of 0.28% indicates a rare occurrence of these conditions in the dataset. Despite this, the high lift value of 353.07 suggests that this combination is a reliable predictor for a significant melt pool area. Furthermore, the strong conviction value also indicates that a big melt pool area (a2) is almost certain when both high image intensity imI2 and high melt pool intensity mpmI1 are observed.

Rule 5, has the highest support value of 55.54%, indicating that it appears in more than half of all transactions in the dataset, making it the most prevalent rule. This high level of support suggests that the pairing of image intensity falling in imI0 and resulting in having the smallest melt pool area is a common event. The confidence of 95% indicates a strong probability that the melt pool area will fall within the size a0 range when the image intensity is in the imI0. Such high confidence indicates a robust correlation between the smallest melt pool area and the darkest images. The lift value suggests a positive correlation is shown between imI0 and a0 clusters. The probability of having the smallest melt pool area increases by a factor of 1.71 when the image intensity is darkest compared to when the image intensity and melt pool area are unrelated. The conviction value of 8.86 indicates that if the relationship between the darkest image intensity (imI0) and smallest melt pool area (a0) were to be disrupted, the probability of imI0 occurring without a0 would decrease by 8.86.

5. DISCUSSION

In this section, we analyze the practical application of the FCA-based methodology for extracting valuable information in AM. We critically assess the accuracy of the resulting association rules across different datasets, particularly focusing on the training layer (layer 21) but also other datasets. The aim is to evaluate the reliability, strength, and validity of the final rules. Furthermore, this will help discuss the limitations of our methodology to provide a comprehensive evaluation of its capabilities and identify areas for future development. Finally, the practical applicability of the rules to guide decisions in the specific context of L-PBF AM is discussed.

5.1 Evaluation of the association rules

To evaluate the reliability of the rules, we analyzed and plotted the variation in confidence error. For each rule, the error variation was determined by calculating the difference between predicted confidence and the actual confidence value, divided by the actual value. The actual confidence was computed as the percentage of data points that validate the rule when the antecedent is verified. A low error variation implies that the rules are generally accurate, with a value of 0 indicating similar values for the observed confidence and the rule's predicted confidence. A negative value suggests that more data points validate the rule, whereas positive values indicate that fewer data points validate the rule.

5.1.1 Melt pool thermal analysis. Figure 6 shows the variation of errors expressed as a percentage, between the expected and observed confidence levels for the final set of rules within the training layer for Melt pool thermal analysis.

For the entire set of rules, the rules were all validated as seen with the small error variation. As we can see, the curve is almost flat across most rules which indicates minimal variation in error. The majority of the rules, from Rule 1 to Rule 12, show very low error percentages suggesting that the predicted confidence is very close to the actual confidence calculated from the data. This shows the model's reliability in predicting the rules across this particular layer. The curve exhibits a small increase in error percentage at Rule 10 which indicates a slight overestimation of the rule's confidence by the model compared to what was observed in the data. This deviation is, however, relatively minor compared to the significant spike appearing in Rule 13 which stands out with the highest error value of 12.5%.This rule exhibits the lowest support with a value of 0.05%, suggesting that it is a relatively rare occurrence within the dataset. The positive error value for this rule suggests that the model's predicted confidence exceeds the actual confidence derived from the data. This relates an overestimation to the few examples of this rule. However, the high lift score signals that the rule, although infrequent, is significant when it does occur. Even so, it is essential to recognize that this rule consistently proves to be validated when its specific conditions are met. Such a contradiction between the model's overestimated confidence and the rule's actual performance suggests that the model may not capture all the subtle conditions under which this rule holds true. Thus, a re-evaluation of the model is necessary to handle this type of rare but important rule. This would ensure that infrequent yet crucial rules are represented more accurately in the predictive analysis.

The plot in Figure 7 displays for all the rules, the variation of errors from the predicted confidence to the real confidence across other datasets for the Melt pool thermal analysis.

As we can see, the plot features three curves representing the error from predicted confidences from layer 21 to the actual confidences from layer 9, layer 33, and layer 69 within the same part. The three curves show different error patterns across the rules. This indicates that the rule's confidence levels are varying from one layer to another, suggesting layer-specific dynamics that could affect the rules' performance. Despite this, the rules were all validated across different datasets.

The curve for Layer 9 shows relatively minor errors until rule 9, suggesting that the majority of the rules are reliable and consistent at this layer. The highest error occurs at rule 13, with a real confidence of 0.05% above the expected confidence of 0.03%. Layer 33 demonstrates moderate errors, which are quite consistent until the last rule, where the absolute value error increases significantly and more data points are found to verify the rules. Layer 69 exhibits the most variability in errors, with the final rules showing a dramatic increase in error percentage. Especially, like for the other layers, rule 13 is found to be validated with more data points verifying the rule. Indeed, the real confidence is at 0.11% while the estimated confidence of the rule scored 0.03%.

Overall, the initial rules show relatively lower error rates until rule 9, which indicates that these rules are robust and have captured generalized patterns in the melt pool data. The final rules for each layer show a pronounced increase in error after rule 9, suggesting that these rules may be less reliable and overfitted to certain conditions that do not hold in layers 9, 33, and 69. The fact that the errors are not consistent after rule 9 for the other layers could imply a challenge in generalizing the rules across different layers for the Melt pool thermal analysis. This may indicate a need for layer-specific adjustments to the rules or the existence of layer-specific phenomena not captured by the current rules. Especially, the increasing absolute error value in later rules, particularly for Layer 69, could suggest that the model might not adequately capture the phenomena at higher layers.

In summary, for the Melt pool thermal analysis, the model performed well in extracting accurate association rules for the analyzed layer. The methodology allowed to extract accurate associations validated with low percentages or errors regarding the confidence for the analyzed layer. Across other datasets, all the rules were also proved valid. However, the rules appear to be more reliable at closer layers as seen in layer 33, and less so at farthest layers. This indicates that while the model has captured certain aspects of the melt pool behavior, there is room for improvement in generalizing the rules across all layers and addressing the variability in the later rules. To enhance the model's performance for multi-layer analysis, further investigation into the layer-specific phenomena and additional refinement of the association rules might be necessary.

5.1.2 Process dynamics and derived melt pool ratio. Figure 8 shows the variation of error from the confidence for layer 21 for the Process dynamics and derived melt pool ratio analysis.

The error curve remains low, suggesting that the rules were validated with confidence levels closely matching their original confidence values. Most rules exhibit error margins within ±2% which indicates reliable predictive capability and good model performance to extract the rules for the training layer. This highlights the model's predictive accuracy in assessing process dynamics and melt pool ratio relationships. The graph is predominantly stable, with no extreme values, except for the last rule. Indeed the most significant error is at 5% with a positive value, implying less data validating the rule 86. This outlier suggests that while the model is generally adept at prediction, it may not consistently capture the intricacies of certain rules, highlighting areas for potential model refinement. Overall, the low error rates indicate the consistency of the rules in terms of reliability for the analyzed layer.

To evaluate the generalizability of the association rules extracted from the Process dynamics and derived melt pool ratio analysis across different layers, Figure 9 provides the real confidences across Layers 9, 33, and 69 for each rule.

Among the 86 rules examined, 10 were not verified at certain layers, which raises questions about the conditions under which these rules were derived or the specific nature of the data at those layers. Conversely, the majority of the rules have been verified across other layers, suggesting a higher level of robustness and potential applicability to other layers.

However, for the rules that were not verified, a deeper investigation into another dimension of the analysis is necessary. This

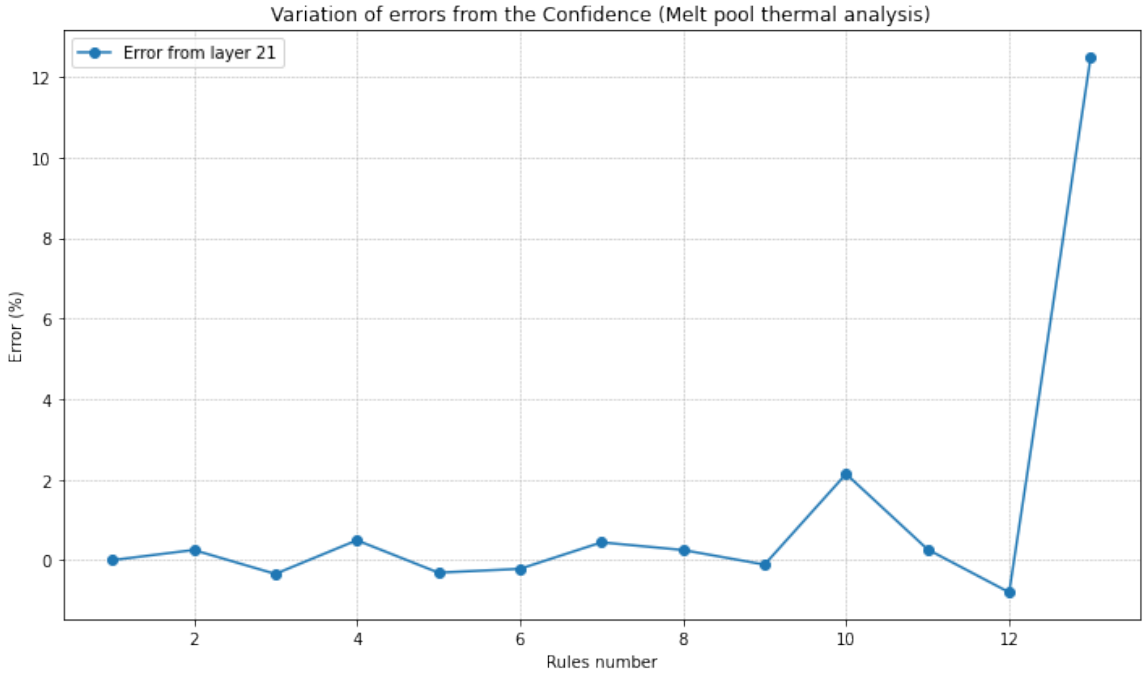

FIGURE 6: Variation of errors from the confidence for all the rules for the training layer (layer 21) for the Melt pool thermal analysis

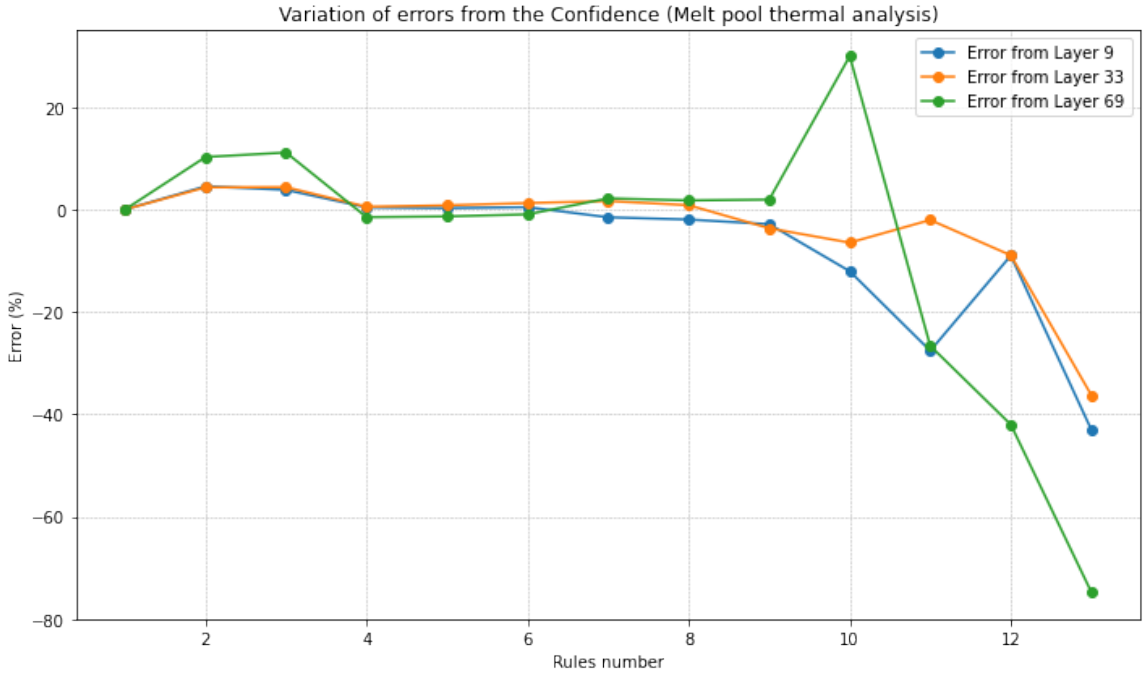

FIGURE 7: Variation of errors from the confidence for all the rules across other layers for the Melt pool thermal analysis

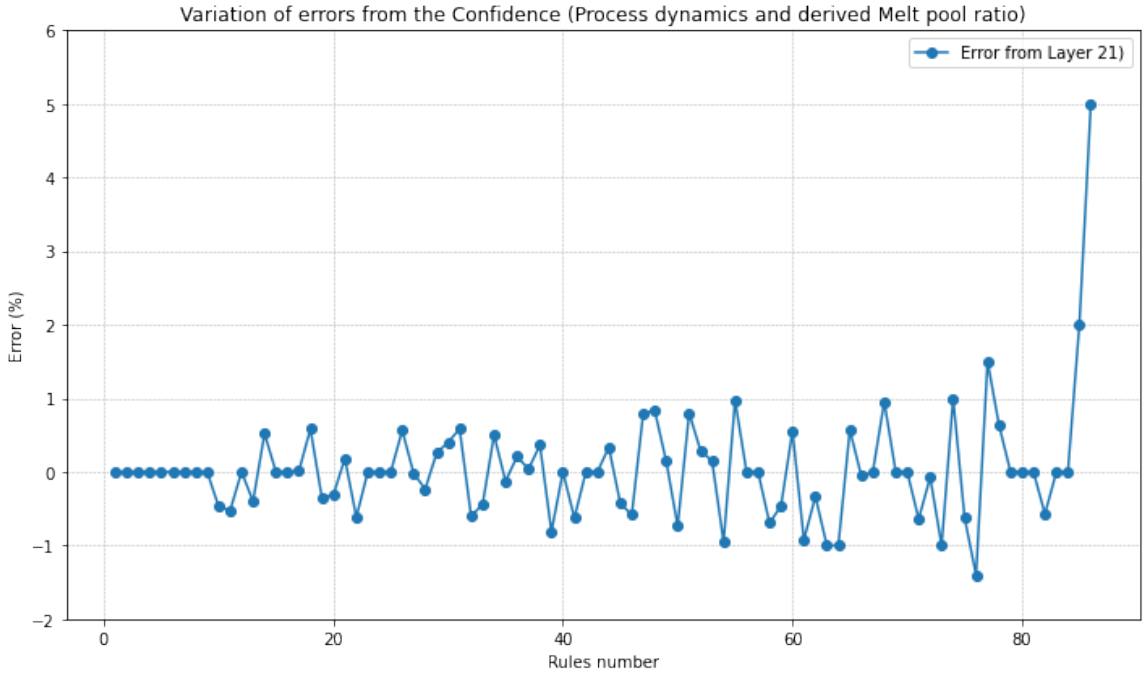

FIGURE 8: Variation of errors from the confidence for all the rules for the training layer (layer 21) for the Process dynamics and derived melt pool ratio analysis

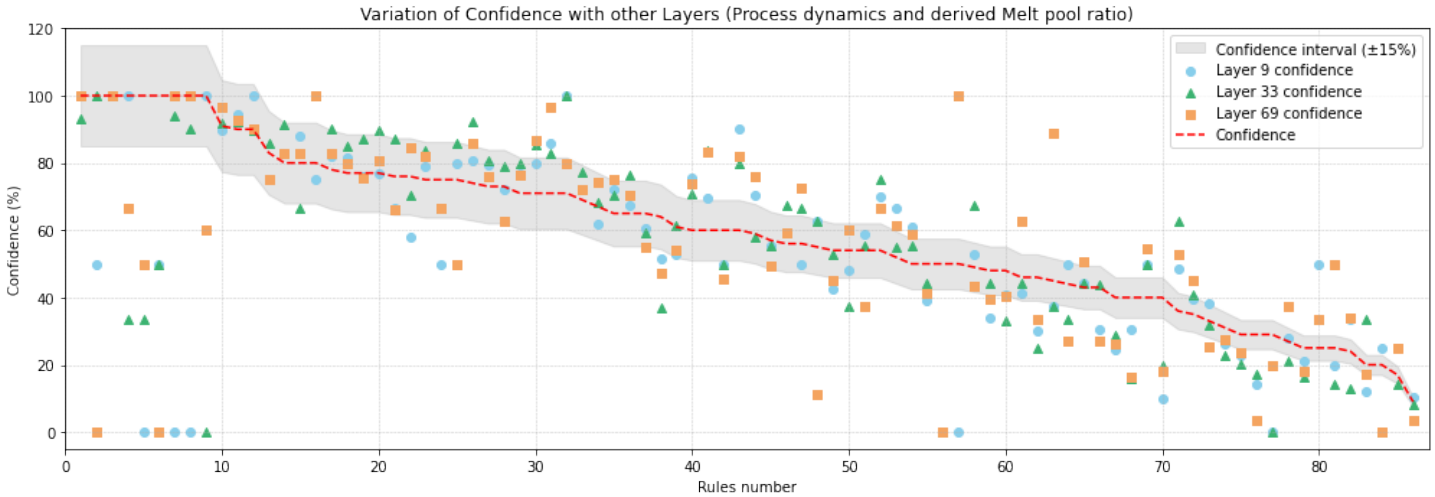

FIGURE 9: Confidence of the rules across other datasets for the Process dynamics and derived melt pool ratio analysis

factor could influence the performance of the rules, particularly if certain datasets have unique characteristics or are subjected to different physical phenomena that are not adequately captured by the existing rules set. Our preliminary hypothesis suggests that the layer level is a significant variable that must be considered. While some rules may be accurate and reliable in certain contexts, their generalization to other layers may be limited without considering the nuances introduced by each distinct layer. This is also observed in Melt pool thermal analysis in which the most significant confidence errors are shown for layer 69 and then layer 9, while layer error rates for layer 33 are minimal.

Overall, when accessing the accuracy of the rules on the training layer, the model demonstrates strong performance, with most rules exhibiting low error variation of the confidence. This indicates reliable predictive capability and underscores the model's accuracy in assessing process dynamics and melt pool ratio relationships for the analyzed layer. Regarding the generalization of the rules to other layers for the same part, the majority of rules have been verified across different layers, suggesting a higher level of robustness and potential applicability. However, further investigation is needed for the rules that were not verified at certain layers, indicating the importance of considering the nuances introduced by each distinct layer for the generalization of rules.

5.2 Practical applicability in Laser-Powder Bed Fusion Additive Manufacturing

The process of extracting association rules using FCA, refining them, and validating their effectiveness for each analysis task demonstrates the robustness of our methodology in deriving reliable and accurate association rules. Although there are minor variations between the predicted and actual confidence levels, this underscores the reliability of the approach. Additionally, all rules were validated across other datasets for Melt pool thermal analysis, with some variations in confidence levels observed. For process dynamics, the majority of the rules (88.37%) were validated, while 10 rules were not validated, indicating the need for further investigation.

The performance of the rules across different layers indicates that while some associations remain consistent, others may vary within the manufacturing environment. This highlights the importance of ongoing research into these rules to fully understand their applicability and reliability in diverse manufacturing settings. Nevertheless, the analysis of confidence with the training layer demonstrates the reliability and consistency of the rules, which could be utilized for decision-making in various scenarios,

With the Process dynamics and derived melt pool ratio analysis, we can conclude that both laser power and laser scan speed have a significant influence on the melt pool ratio. Specific combinations of these parameters can lead to predictable outcomes, with higher settings generally associated with smaller melt pool ratios and lower settings also leading to smaller melt pools in some cases. Certain combinations are common in the dataset and have a moderate influence on the melt pool ratio. The rules obtained for this analysis can be applied in several situations to enhance AM processes. Indeed we believe that the rules could be used for real-time monitoring of the melt pool to make spontaneous adjustments to the process parameters and ensure that the melt pool size remains within the desired range. This could lead to optimal print quality and reduce the possibility of defects. Additionally, the rules can be employed for predictive maintenance by identifying inconsistencies in melt pool sizes that may indicate equipment issues. The rules could also serve for quality control to establish specific parameters that ensure consistently high-quality parts. By serving as guidelines, these rules could help manufacturers maintain a standard level of quality across similar produced parts which could reduce the need for post-processing and part rebuilding. Finally, process optimization for similar part designs can be achieved to fine-tune process settings and ensure the desired melt pool characteristics are met.

The rules derived from the Melt Pool Thermal Analysis establish a comprehensive structure of connections that specify the relationships between different images and melt pool intensities and the size of the melt pool.

The rules could be useful for predicting melt pool areas based on melt pool and image intensities when collecting MPM images. The obtained rules could also be used for real-time monitoring in AM processes allowing for adjustments based on the detected image and melt pool intensities to maintain the desired melt pool area size. Furthermore, the set of rules could be used to detect melting anomalies. For instance, from rule 1 if a melt pool is detected in normal printing, high image, and melt pool intensities should be correlated with a melt pool area within the range of a2. In this specific scenario of having a melt pool detected with high melt pool and image intensities, if the melt pool area does not range from 0.041152 mm^2 to 0.082432 mm^2, rule 1 is violated. This transgression of the rule could indicate a certain anomaly in the printing process. From this, the operator could stop the build to avoid part failure.

5.3 Limitations

The proposed approach allowed to extract association rules that could be used in different scenarios depending on the analyzed parameters from the AM multi-modal data. However, the application of our methodology to AM multi-modal data highlights its constraints, notably the inconsistency in rule confidence levels across other layers.

The minimal error rates seen in the rules analysis for layer 33 can be attributed to its proximity to layer 21. This suggests that the physical properties of layer 21 are more closely reflected in layer 33 compared to the other layers analyzed. Moreover, discrepancies in rule validation across datasets point to the influence of layer positioning within the build structure on the results. We can speculate that the layer level itself may have a significant impact on the rules' confidence. Thus, further investigation into the layer-specific conditions that cause discrepancies in rule verification will be essential in refining the rules for enhanced accuracy and broader applicability than the analyzed layer. In this aim, incorporating Relational Concept Analysis (RCA) [42], which considers object-attributes relationships and not only attributes-attributes connections, could help us include the layer level in the analysis and extract association rules with this multidimensional aspect. This would ensure that the rules are generalized with the correct confidence levels across other layers and not only the training set.

For the Process dynamics and derived melt pool ratio, as seen, some of the rules were not validated across other layers. We strongly suspect that the layer level once again plays a crucial role here. However, we also believe that certain rules failed to be validated due to the initial cluster boundaries set by the clustering method used. The sensitivity of the methodology to boundary definition may affect rule validation and needs to be examined for potential improvements. The disparity in cluster distribution suggests that the K-means clustering technique may not effectively capture the intricacies of AM data consistently. Therefore, exploring different data ranges but also different clustering methods could improve the understanding of AM multi-modal data relationships and enhance rule accuracy. In this aim, domain knowledge from the literature could be incorporated to more accurately cluster individual sets of parameters especially for melt pool features. Another solution could be to reduce the dependency on Machine Learning classification boundaries, which can add over-fitting or under-fitting issues. For this, techniques such as using fuzzy logic could offer a more nuanced approach [43]. Fuzzy sets could indeed accommodate the natural variability in the data, allowing for softer transitions between clusters and reflecting the real-world ambiguity in the categorization of the numerical data. This could potentially enhance the precision and robustness of the rules extracted.

As we saw with the Process dynamics and derived melt pool ratio, the set of extracted rules could remain extensive. Making use of such a large number of rules can be difficult for operators or automated systems to efficiently manage and apply in real-time. To enhance usability it is necessary to reduce the number of rules. This could involve identifying the most influential and consistent rules that are critical for maintaining quality and stability in the AM process. By streamlining the rule set, we could improve the decision-making process. The goal is to balance the comprehensiveness of the data with practical application, ensuring that the insights derived from the rules are both actionable and manageable within the operational workflow. In this aim, pruning algorithms will be explored to decrease the number of redundant rules. Using this approach, we aim to decrease the number of rules but also improve the reliability and comprehensiveness of the extracted rules.

6. CONCLUSION

This research introduces a new methodology for knowledge extraction in Laser-Powder Bed Fusion (L-PBF) Additive Manufacturing (AM). The methodology combines Formal Concept Analysis (FCA), which has not been previously investigated in the realm of AM, with data processing techniques and Machine Learning (ML) algorithms to derive association rules for AM in-process monitoring. These rules are then refined through Rules engineering and used for process control. Beyond the traditional metrics used in FCA, additional metrics such as lift and conviction were incorporated to assess the strength and reliability of the extracted rules. The methodology allowed us to identify and validate valuable association rules derived from Melt Pool Monitoring (MPM) images captured from normal operations. These rules can guide in-process decision-making, for example, detecting anomalies, adjust process settings or stop a build. We were able to uncover relationships between laser power, laser scan speed, and melt pool ratio, as well as those between melt pool intensity and melt pool area. Additionally, we examined the correlation between specific ranges of process parameter values and ranges of melt pool feature values, which enhances our understanding of their interplay in the AM process.

Future work will focus on enhancing this methodology by discovering the dependency of the relationships on the layer number, streamlining the rules, and formalizing them into an ontology. This will expand the applicability of the approach and ensure their relevance for decision-making in the rapidly evolving field of AM.

DISCLAIMER

Certain commercial systems are identified in this paper. Such identification does not imply recommendation or endorsement by NIST; nor does it imply that the products identified are necessarily the best available for the purpose. Further, any opinions, findings, conclusions, or recommendations expressed in this material are those of the authors and do not necessarily reflect the views of NIST or any other supporting U.S. government or corporate organizations.

REFERENCES

[1] Frazier, William E. "Metal additive manufacturing: a review." *Journal of Materials Engineering and performance* Vol. 23 (2014): pp. 1917–1928.

[2] Oliveira, João Pedro, LaLonde, AD and Ma, J. "Processing parameters in laser powder bed fusion metal additive manufacturing." *Materials & Design* Vol. 193 (2020): p. 108762.

[3] Mani, Mahesh, Feng, Shaw, Brandon, Lane, Donmez, Alkan, Moylan, Shawn and Fesperman, Ronnie. "Measurement science needs for real-time control of additive manufacturing powder-bed fusion processes." *Additive manufacturing handbook*. CRC Press (2017): pp. 629–652.

[4] McCann, Ronan, Obeidi, Muhannad A, Hughes, Cian, McCarthy, Éanna, Egan, Darragh S, Vijayaraghavan, Rajani K, Joshi, Ajey M, Garzon, Victor Acinas, Dowling, Denis P, McNally, Patrick J et al. "In-situ sensing, process monitoring and machine control in Laser Powder Bed Fusion: A review." *Additive Manufacturing* Vol. 45 (2021): p. 102058.

[5] Wang, Chengcheng, Tan, Xipeng P, Tor, Shu Beng and Lim, CS. "Machine learning in additive manufacturing: State-of-the-art and perspectives." *Additive Manufacturing* Vol. 36 (2020): p. 101538.

[6] Yeung, Ho, Yang, Zhuo and Yan, L. "A meltpool prediction based scan strategy for powder bed fusion additive manufacturing." *Additive Manufacturing* Vol. 35 (2020): p. 101383.

[7] Scime, Luke and Beuth, Jack. "Anomaly detection and classification in a laser powder bed additive manufacturing process using a trained computer vision algorithm." *Additive Manufacturing* Vol. 19 (2018): pp. 114–126. DOI https://doi.org/10.1016/j.addma.2017.11.009.

[8] Kim, Jaehyuk, Yang, Zhuo, Ko, Hyunwoong, Cho, Hyunbo and Lu, Yan. "Deep learning-based data registration of melt-pool-monitoring images for laser powder bed fusion additive

manufacturing." *Journal of Manufacturing Systems* Vol. 68 (2023): pp. 117–129.

[9] Carraturo, Massimo and Mazzullo, Andrea. "An Ontology for Defect Detection in Metal Additive Manufacturing." *arXiv preprint arXiv:2210.04772* (2022).

[10] Yang, Zhuo, Lu, Yan, Li, Simin, Li, Jennifer, Ndiaye, Yande, Yang, Hui and Krishnamurty, Sundar. "In-process data fusion for process monitoring and control of metal additive manufacturing." *International Design Engineering Technical Conferences and Computers and Information in Engineering Conference*, Vol. 85376: p. V002T02A072. 2021. American Society of Mechanical Engineers.

[11] Cutrona, L., Leith, E., Palermo, C. and Porcello, L. "Optical data processing and filtering systems." *IRE Transactions on Information Theory* Vol. 6 No. 3 (1960): pp. 386–400. DOI 10.1109/TIT.1960.1057566.

[12] Khalid, Samina, Khalil, Tehmina and Nasreen, Shamila. "A survey of feature selection and feature extraction techniques in machine learning." *2014 Science and Information Conference*: pp. 372–378. 2014. DOI 10.1109/SAI.2014.6918213.

[13] Berkhin, Pavel. "A survey of clustering data mining techniques." *Grouping multidimensional data: Recent advances in clustering*. Springer (2006): pp. 25–71.

[14] Adnan, Muhammad, Lu, Yan, Jones, Albert, Cheng, Fan-Tien and Yeung, Ho. "A new architectural approach to monitoring and controlling AM processes." *Applied Sciences* Vol. 10 No. 18 (2020): p. 6616.

[15] Zhang, Siqi, Lu, Yan and Yang, Hui. "Multiscale basis modeling of 3D melt-pool morphological variations for manufacturing process monitoring." *The International Journal of Advanced Manufacturing Technology* (2024): pp. 1–12.

[16] Ganter, Bernhard and Wille, Rudolf. *Formal Concept Analysis*. Springer Berlin and Heidelberg (1999). DOI https://doi.org/10.1007/978-3-642-59830-2.

[17] Ganter, Bernhard, Stumme, Gerd and Wille, Rudolf. *Formal concept analysis: foundations and applications*. Vol. 3626. springer (2005).

[18] Poelmans, Jonas, Ignatov, Dmitry I, Kuznetsov, Sergei O and Dedene, Guido. "Formal concept analysis in knowledge processing: A survey on applications." *Expert systems with applications* Vol. 40 No. 16 (2013): pp. 6538–6560.

[19] Ferré, Sébastien, Huchard, Marianne, Kaytoue, Mehdi, Kuznetsov, Sergei O and Napoli, Amedeo. "Formal concept analysis: from knowledge discovery to knowledge processing." *A Guided Tour of Artificial Intelligence Research: Volume II: AI Algorithms* (2020): pp. 411–445.

[20] Ganter, Bernhard and Wille, Rudolf. "Mathematical Foundations." *Formal Concept Analysis*. 2012. Springer Berlin Heidelberg, Berlin, Heidelberg. DOI https://doi.org/10.1007/978-3-642-59830-2.

[21] Ganter, B. "Two Basic Algorithms in Concept Analysis." Kwuida, L. and Sertkaya, B. (eds.). *Formal Concept Analysis. ICFCA 2010. Lecture Notes in Computer Science*, Vol. 5986: pp. ??–?? 2010. Springer, Berlin, Heidelberg. DOI https://doi.org/10.1007/978-3-642-11928-6_22.

[22] Andrews, S. "In-Close, a fast algorithm for computing formal concepts." *International Conference on Conceptual Structures (ICCS)*. 2009. URL http://iccs09.hse.ru/index.html. Final version of paper accepted (via peer review) for the International Conference on Conceptual Structures (ICCS) 2009, Moscow.

[23] Wille, Rudolf. "Restructuring lattice theory: An approach based on hierarchies of concepts." Rival, Ivan (ed.). *Ordered Sets. Proceedings of the NATO Advanced Study Institute held at Banff, Canada, August 28 to September 12, 1981*, Vol. 83: pp. 445–470. 1982. Springer. DOI 10.1007/978-94-009-7798-3.

[24] Kumbhare, Trupti A. and Chobe, Santosh V. "An overview of association rule mining algorithms." *International Journal of Computer Science and Information Technologies* Vol. 5 No. 1 (2014): pp. 927–930.

[25] Agrawal, Rakesh and Srikant, Ramakrishnan. "Fast algorithms for mining association rules." *Proc. 20th int. conf. very large data bases, VLDB*, Vol. 1215: pp. 487–499. 1994.

[26] Han, Jiawei, Pei, Jian and Yin, Yiwen. "Mining Frequent Patterns without Candidate Generation." *SIGMOD Rec.* Vol. 29 No. 2 (2000): p. 1–12. DOI 10.1145/335191.335372. URL https://doi.org/10.1145/335191.335372.

[27] Nath, Bhabesh, Bhattacharyya, Dhruba K. and Ghosh, Ashish. "Incremental association rule mining: a survey." *Wiley Interdisciplinary Reviews: Data Mining and Knowledge Discovery* Vol. 3 No. 3 (2013): pp. 157–169.

[28] Lane, B., Mekhontsev, S., Grantham, S., Vlasea, M. L., Whiting, J., Yeung, H., Fox, J., Zarobila, C., Neira, J., McGlauflin, M., Moylan, L. Hanssen S., Donmez, A. and Rice, J. "Design, Developments, and Results from the NIST Additive Manufacturing Metrology Testbed (AMMT)." *Proceedings of the Solid Freeform Fabrication Symposium* (2016).

[29] Lane, Brandon and Yeung, Ho. "Process Monitoring Dataset from the Additive Manufacturing Metrology Testbed (AMMT): Three-Dimensional Scan Strategies." (2019)DOI https://doi.org/10.6028/jres.124.033.

[30] Likas, Aristidis, Vlassis, Nikos and Verbeek, Jakob J. "The global k-means clustering algorithm." *Pattern Recognition* Vol. 36 (2003): pp. 451–461. DOI 10.1016/S0031-3203(02)00060-2. URL https://www.sciencedirect.com/science/article/pii/S0031320302000602.

[31] Rousseeuw, Peter J. "Silhouettes: A graphical aid to the interpretation and validation of cluster analysis." *Journal of Computational and Applied Mathematics* Vol. 20 (1987): pp. 53–65. DOI 10.1016/0377-0427(87)90125-7. URL https://www.sciencedirect.com/science/article/pii/0377042787901257.

[32] "Repository and documention for ConExp tool." URL https://conexp.sourceforge.net/.

[33] Narasimharaju, Shubhavardhan Ramadurga, Zeng, Wenhan, See, Tian Long, Zhu, Zicheng, Scott, Paul, Jiang, Xiangqian and Lou, Shan. "A comprehensive review on laser powder bed fusion of steels: Processing, microstructure, defects and

control methods, mechanical properties, current challenges and future trends." *Journal of Manufacturing Processes* Vol. 75 (2022): pp. 375–414.

[34] Cheng, Bo, Lydon, James, Cooper, Kenneth, Cole, Vernon, Northrop, Paul and Chou, Kevin. "Melt pool sensing and size analysis in laser powder-bed metal additive manufacturing." *Journal of Manufacturing Processes* Vol. 32 (2018): pp. 744–753.

[35] Criales, Luis E, Arısoy, Yiğit M, Lane, Brandon, Moylan, Shawn, Donmez, Alkan and Özel, Tuğrul. "Laser powder bed fusion of nickel alloy 625: Experimental investigations of effects of process parameters on melt pool size and shape with spatter analysis." *International Journal of Machine Tools and Manufacture* Vol. 121 (2017): pp. 22–36.

[36] Zhang, Bi, Li, Yongtao and Bai, Qian. "Defect formation mechanisms in selective laser melting: a review." *Chinese Journal of Mechanical Engineering* Vol. 30 (2017): pp. 515–527.

[37] Gong, Haijun, Rafi, Khalid, Gu, Hengfeng, Starr, Thomas and Stucker, Brent. "Analysis of defect generation in Ti–6Al–4V parts made using powder bed fusion additive manufacturing processes." *Additive Manufacturing* Vol. 1 (2014): pp. 87–98.

[38] Kryszkiewicz, M. "Concise Representations of Association Rules." Hand, D.J., Adams, N.M. and Bolton, R.J. (eds.). *Pattern Detection and Discovery*. Vol. 2447 of *Lecture Notes in Computer Science*. Springer, Berlin, Heidelberg (2002). DOI 10.1007/3-540-45728-3_8. URL https://doi.org/10.1007/3-540-45728-3_8.

[39] Lakhal, L. and Stumme, G. "Efficient Mining of Association Rules Based on Formal Concept Analysis." Ganter, B., Stumme, G. and Wille, R. (eds.). *Formal Concept Analysis*. Vol. 3626 of *Lecture Notes in Computer Science*. Springer, Berlin, Heidelberg (2005). DOI 10.1007/11528784_10. URL https://doi.org/10.1007/11528784_10.

[40] McNicholas, Paul D., Murphy, Thomas Brendan and O'Regan, Michael. "Standardising the lift of an association rule." *Computational Statistics & Data Analysis* Vol. 52 No. 10 (2008): pp. 4712–4721. DOI 10.1016/j.csda.2008.03.013. URL https://www.sciencedirect.com/science/article/pii/S0167947308001709.

[41] Brin, Sergey, Motwani, Rajeev, Ullman, Jeffrey D and Tsur, Shalom. "Dynamic itemset counting and implication rules for market basket data." *SIGMOD Record* Vol. 26 No. 2 (1997): pp. 255–264.

[42] Rouane-Hacene, Mehdi, Huchard, Marianne, Napoli, Amedeo et al. "Relational concept analysis: mining concept lattices from multi-relational data." *Annals of Mathematics and Artificial Intelligence* Vol. 67 (2013): pp. 81–108. DOI 10.1007/s10472-012-9329-3.

[43] Li, Jiamin and Lewis, Harold W. "Fuzzy clustering algorithms—review of the applications." *2016 IEEE International Conference on Smart Cloud (SmartCloud)*: pp. 282–288. 2016. IEEE.

[44] Grasso, Marco and Colosimo, Bianca Maria. "Process defects and in situ monitoring methods in metal powder bed fusion: a review." *Measurement Science and Technology* Vol. 28 No. 4 (2017): p. 044005.

[45] Azevedo, Paulo J and Jorge, Alípio M. "Comparing rule measures for predictive association rules." *European Conference on Machine Learning*: pp. 510–517. 2007. Springer.

[46] Lu, Yan, Yang, Zhuo, Kim, Jaehyuk, Cho, Hyunbo and Yeung, Ho. "CAMERA-BASED COAXIAL MELT POOL MONITORING DATA REGISTRATION FOR LASER POWDER BED FUSION ADDITIVE MANUFACTURING." (2020).

APPENDIX A. PART OF THE CSV FILE CREATED AFTER FEATURES EXTRACTION

	x(mm)	y(mm)	P(W)	v(mm/s)	length(mm)	width(mm)	area(mm^2)	ratio	image intensity	meltpool intensity
p1	**14.017**	-20.457	83.4	500.000000000078	0.145587084821361	0.109143053103569	0.012608	1.33391068585199	7.51419270833333	160.737373737374
p2	**13.694**	-20.4	102.95	905.538513813612	0.152566717561155	0.100274001755201	0.012096	1.5214982437184	7.6396484375	173.859375
p3	**13.253**	-20.322	105.0	905.538513813789	0.142989248334386	0.0910968197346187	0.010304	1.56964039744679	7.29850260416667	164.621118012422
p4	**12.81**	-20.244	105.0	905.538513813789	0.150990055741153	0.09127172352884	0.01088	1.65429171164323	7.3873046875	165.7
p5	**12.367**	-20.165	105.0	921.954445729202	0.157924247825523	0.0992734881157799	0.012544	1.59079982806024	7.81770833333333	170.944444444444
p6	**11.924**	-20.087	105.0	824.621125123592	0.144685325002835	0.0912580357952369	0.01056	1.58545298221712	7.62858072916667	161.958823529412
p7	**11.48**	-20.009	105.0	921.954445729298	0.145298456017049	0.0939776728371124	0.01088	1.5460954887539	7.38313802083333	168.860465116279
p8	**11.037**	-19.931	105.0	921.954445729125	0.155756842550071	0.0917526081916583	0.011328	1.69757400492329	7.598828125	165.234636871508
p9	**10.594**	-19.853	105.0	905.53851381375	0.142772094026142	0.0947901562282048	0.010752	1.50619114586563	7.3798828125	168.658823529412
p10	**10.151**	-19.775	105.0	905.538513813789	0.159224939883823	0.0961852068655335	0.012096	1.65539946393647	7.88984375	169.636842105263
p11	**9.7084**	-19.697	104.49	875.728268357374	0.16998030938027	0.0948910844688848	0.012608	1.79132012592824	8.17955729166667	173.678391959799
p12	**9.3553**	-19.634	85.394	509.901951359379	0.168065338198403	0.103109874138151	0.013696	1.6299635665661	8.2283203125	181.283720930233
p13	**9.2**	-19.52	82.687	400.000000000134	0.164015585195291	0.100806578636273	0.01312	1.6270325549594	7.91731770833333	180.339805825243
p14	**9.2**	-19.22	100.41	800.000000000267	0.15401646958928	0.102901787891536	0.012352	1.49673268798421	7.70403645833333	174.5
p15	**9.2**	-18.777	105.01	900.000000000034	0.141553775861287	0.088047439236744	0.009728	1.60769895284148	7.7013671875	168.467948717949
...	...	...	...	...	...	...	...	...	...	...
p3413	**16.589**	-18.83	211.45	608.276253029865	0.224685777636883	0.166281391915074	0.02944	1.35123825371656	13.5583984375	182.385438972163
..		...	...	...	...	...	...	...	...	...
p4942	**13.208**	-20.314	165.75	509.901951359379	0.192362946180665	0.130093824930623	0.019712	1.47864778580574	9.90481770833333	187.776699029126

FIGURE 10: Part of the CSV table generated after features extraction

APPENDIX B. PART OF THE GENERATED LATTICE FOR THE MELT POOL THERMAL ANALYSIS

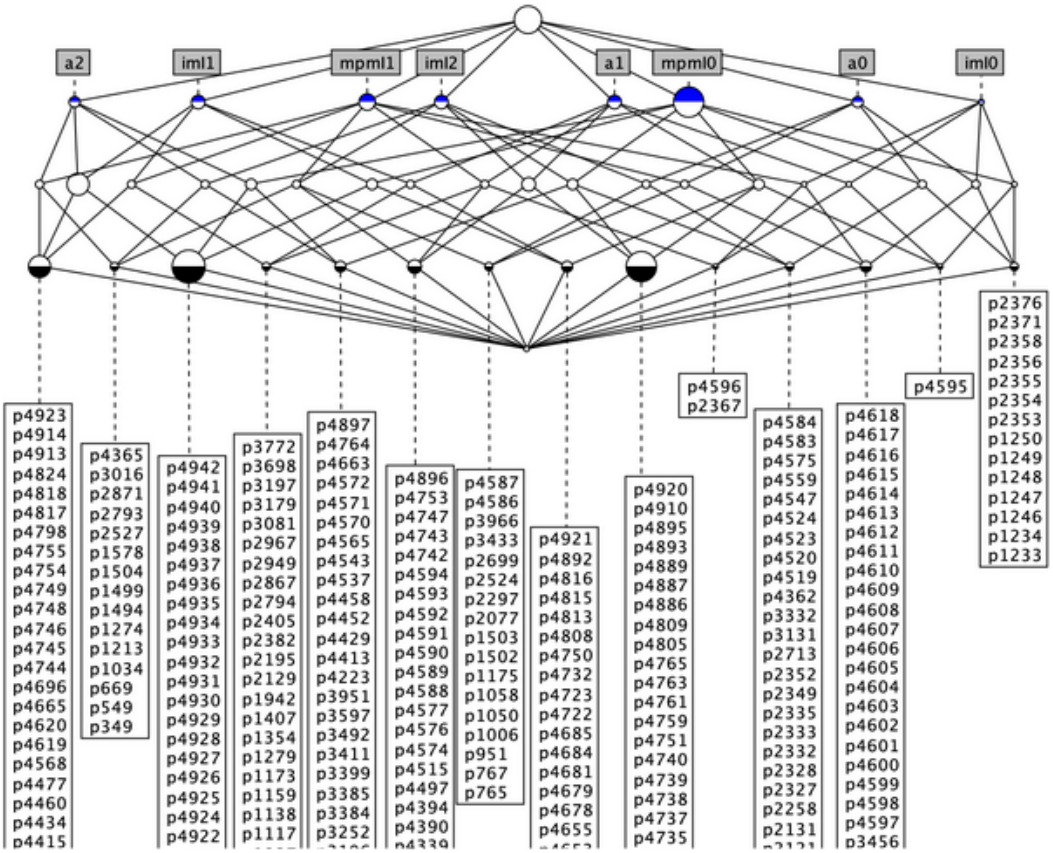

FIGURE 11: Part of the *lattice* produced for Melt pool thermal analysis

APPENDIX C. CLUSTERS INFORMATION

TABLE 3: Clusters information for Laser Power

Cluster name	Cluster size	Range of values (W)
P0	48	[60.025;93.358]
P1	152	[93.962;110.65]
P2	527	[117.04;134.16]
P3	308	[134.26;148.34]
P4	1374	[148.51;158.5]
P5	301	[160.61;165.79]
P6	538	[182.14;200.89]
P7	287	[201.05;222.29]
P8	1408	[222.76;234.77]

TABLE 4: Clusters information for Melt Pool Area

Cluster name	Cluster size	Range of values (mm^2)
a0	2845	[0.0; 0.02464]
a1	1959	[0.024704; 0.040832]
a2	139	[0.041152; 0.082432]

TABLE 5: Clusters information for Laser Scan Speed

Cluster name	Cluster size	Range of values (mm/s)
v1	140	[260.00000000005; 373.630833845468]
v2	789	[378.021163428723; 456.179789118488]
v3	610	[459.999999999994; 539.351462406437]
v4	333	[554.616984954381; 640.312423743568]
v5	566	[659.999999999883; 740.000000000052]
v6	2359	[761.577310586365; 848.528137423889]
v7	125	[875.728268357374; 999.999999999979]

TABLE 6: Clusters information for Melt Pool ratio

Cluster name	Cluster size	Range of values
r0	2988	[0.0; 1.46556088621456]
r1	1955	[1.46594470346874; 2.94406770833032]

TABLE 7: Clusters information for Melt Pool Intensity

Cluster name	Cluster size	Range of values
mpmI0	1128	[0.0;177.233962264151]
mpmI1	3815	[177.25;204.086440677966]

TABLE 8: Clusters information for Image Intensity

Cluster name	Cluster size	Range of values
imI0	2891	[0.0;11.5439453125]
imI1	1963	[11.5471354166667; 18.3029947916667]
imI2	89	[18.4022786458333; 29.8227864583333]

APPENDIX D. FINAL SET OF ASSOCIATION RULES FOR THE MELT POOL THERMAL ANALYSIS

1. Rule: imI2, mpmI1 → a2, Support: 0.28%, Confidence: 100%, Lift: 353.07, Conviction: 1e+10
2. Rule: imI2 → a2, Support: 1.76%, Confidence: 98.00%, Lift: 55.68, Conviction: 49.12
3. Rule: imI2, mpmI0 → a2, Support: 1.47%, Confidence: 97.00%, Lift: 65.68, Conviction: 32.84
4. Rule: imI0, mpmI0 → a0, Support: 15.61%, Confidence: 96.00%, Lift: 6.18, Conviction: 21.12
5. Rule: imI0 → a0, Support: 55.54%, Confidence: 95.00%, Lift: 1.71, Conviction: 8.86
6. Rule: imI0, mpmI1 → a0, Support: 40.09%, Confidence: 95.00%, Lift: 2.36, Conviction: 11.96
7. Rule: imI1, mpmI1 → a1, Support: 32.61%, Confidence: 94.00%, Lift: 2.89, Conviction: 11.25
8. Rule: imI1 → a1, Support: 36.93%, Confidence: 93.00%, Lift: 2.52, Conviction: 9.02
9. Rule: imI1, mpmI0 → a1, Support: 4.36%, Confidence: 87.00%, Lift: 19.91, Conviction: 7.36
10. Rule: mpmI0 → a1, Support: 5.24%, Confidence: 23.00%, Lift: 4.48, Conviction: 1.23
11. Rule: mpmI0 → a2, Support: 1.82%, Confidence: 8.00%, Lift: 4.39, Conviction: 1.07
12. Rule: imI1, mpmI0 → a0, Support: 0.30%, Confidence: 6.00%, Lift: 19.77, Conviction: 1.06
13. Rule: imI2, mpmI0 → a1, Support: 0.05%, Confidence: 3.00%, Lift: 74.14, Conviction: 1.03

APPENDIX E. FINAL SET OF ASSOCIATION RULES FOR THE PROCESS DYNAMICS AND DERIVED MELT POOL RATIO ANALYSIS

1. Rule: P3, v1 → r0, Support: 0.26%, Confidence: 100.00%, Lift: 380.23, Conviction: 1e+10
2. Rule: P2, v5 → r0, Support: 0.10%, Confidence: 100.00%, Lift: 988.60, Conviction: 1e+10
3. Rule: P2, v0 → r0, Support: 0.06%, Confidence: 100.00%, Lift: 1647.67, Conviction: 1e+10
4. Rule: P0, v1 → r0, Support: 0.04%, Confidence: 100.00%, Lift: 2471.50, Conviction: 1e+10
5. Rule: P4, v7 → r1, Support: 0.04%, Confidence: 100.00%, Lift: 2471.50, Conviction: 1e+10
6. Rule: P0, v5 → r1, Support: 0.02%, Confidence: 100.00%, Lift: 4943.00, Conviction: 1e+10
7. Rule: P1, v0 → r0, Support: 0.02%, Confidence: 100.00%, Lift: 4943.00, Conviction: 1e+10
8. Rule: P4, v0 → r0, Support: 0.02%, Confidence: 100.00%, Lift: 4943.00, Conviction: 1e+10
9. Rule: P6, v6 → r0, Support: 0.02%, Confidence: 100.00%, Lift: 4943.00, Conviction: 1e+10
10. Rule: P4, v2 → r0, Support: 0.64%, Confidence: 91.00%, Lift: 140.57, Conviction: 11.04
11. Rule: v0 → r0, Support: 0.38%, Confidence: 90.00%, Lift: 234.14, Conviction: 9.96
12. Rule: P3, v0 → r0, Support: 0.18%, Confidence: 90.00%, Lift: 494.30, Conviction: 9.98
13. Rule: P0, v0 → r0, Support: 0.10%, Confidence: 83.00%, Lift: 820.54, Conviction: 5.88
14. Rule: P2, v2 → r0, Support: 5.47%, Confidence: 80.00%, Lift: 14.70, Conviction: 4.73
15. Rule: P5, v2 → r0, Support: 0.40%, Confidence: 80.00%, Lift: 197.72, Conviction: 4.98
16. Rule: P5, v6 → r0, Support: 0.08%, Confidence: 80.00%, Lift: 988.60, Conviction: 5.00
17. Rule: P2 → r0, Support: 8.32%, Confidence: 78.00%, Lift: 9.38, Conviction: 4.17
18. Rule: v2 → r0, Support: 12.29%, Confidence: 77.00%, Lift: 6.30, Conviction: 3.82
19. Rule: P3 → r0, Support: 4.80%, Confidence: 77.00%, Lift: 15.99, Conviction: 4.14
20. Rule: P3, v4 → r0, Support: 2.26%, Confidence: 77.00%, Lift: 33.98, Conviction: 4.25
21. Rule: P3, v3 → r0, Support: 0.89%, Confidence: 76.00%, Lift: 85.38, Conviction: 4.13
22. Rule: P0, v3 → r0, Support: 0.26%, Confidence: 76.00%, Lift: 288.98, Conviction: 4.16
23. Rule: P2, v3 → r0, Support: 1.76%, Confidence: 75.00%, Lift: 42.61, Conviction: 3.93
24. Rule: P8, v7 → r1, Support: 0.06%, Confidence: 75.00%, Lift: 1235.75, Conviction: 4.00
25. Rule: P1, v5 → r0, Support: 0.06%, Confidence: 75.00%, Lift: 1235.75, Conviction: 4.00
26. Rule: P2, v1 → r0, Support: 0.79%, Confidence: 74.00%, Lift: 93.79, Conviction: 3.82
27. Rule: P6, v2 → r0, Support: 5.58%, Confidence: 73.00%, Lift: 13.07, Conviction: 3.50
28. Rule: P3, v5 → r0, Support: 1.21%, Confidence: 73.00%, Lift: 60.14, Conviction: 3.66
29. Rule: P6 → r0, Support: 7.73%, Confidence: 71.00%, Lift: 9.21, Conviction: 3.18

30. Rule: v1 → r0, Support: 2.01%, Confidence: 71.00%, Lift: 35.45, Conviction: 3.38
31. Rule: P4, v1 → r0, Support: 0.24%, Confidence: 71.00%, Lift: 292.46, Conviction: 3.44
32. Rule: P2, v6 → r0, Support: 0.10%, Confidence: 71.00%, Lift: 701.91, Conviction: 3.44
33. Rule: P6, v3 → r0, Support: 1.41%, Confidence: 69.00%, Lift: 48.72, Conviction: 3.18
34. Rule: P0 → r0, Support: 0.65%, Confidence: 67.00%, Lift: 103.49, Conviction: 3.01
35. Rule: v3 → r0, Support: 8.01%, Confidence: 65.00%, Lift: 8.11, Conviction: 2.63
36. Rule: v4 → r0, Support: 4.38%, Confidence: 65.00%, Lift: 14.87, Conviction: 2.73
37. Rule: P4, v5 → r0, Support: 2.59%, Confidence: 65.00%, Lift: 25.10, Conviction: 2.78
38. Rule: P7, v5 → r1, Support: 0.89%, Confidence: 64.00%, Lift: 71.90, Conviction: 2.75
39. Rule: P4 → r0, Support: 16.96%, Confidence: 61.00%, Lift: 3.57, Conviction: 2.13
40. Rule: P7, v3 → r0, Support: 0.73%, Confidence: 60.00%, Lift: 82.38, Conviction: 2.48
41. Rule: P6, v1 → r0, Support: 0.64%, Confidence: 60.00%, Lift: 92.68, Conviction: 2.48
42. Rule: P6, v4 → r1, Support: 0.06%, Confidence: 60.00%, Lift: 988.60, Conviction: 2.50
43. Rule: P2, v4 → r0, Support: 0.06%, Confidence: 60.00%, Lift: 988.60, Conviction: 2.50
44. Rule: P5 → r0, Support: 3.58%, Confidence: 59.00%, Lift: 16.57, Conviction: 2.35
45. Rule: v5 → r0, Support: 6.53%, Confidence: 57.00%, Lift: 8.70, Conviction: 2.17
46. Rule: P7, v4 → r0, Support: 1.79%, Confidence: 56.00%, Lift: 31.10, Conviction: 2.23
47. Rule: P0, v4 → r0, Support: 0.10%, Confidence: 56.00%, Lift: 553.62, Conviction: 2.27
48. Rule: P5, v4 → r1, Support: 0.12%, Confidence: 55.00%, Lift: 453.11, Conviction: 2.22
49. Rule: v6 → r0, Support: 25.77%, Confidence: 54.00%, Lift: 2.10, Conviction: 1.61
50. Rule: v7 → r1, Support: 1.37%, Confidence: 54.00%, Lift: 39.25, Conviction: 2.14
51. Rule: P1, v6 → r0, Support: 0.31%, Confidence: 54.00%, Lift: 177.95, Conviction: 2.17
52. Rule: P0, v2 → r0, Support: 0.14%, Confidence: 54.00%, Lift: 381.32, Conviction: 2.17
53. Rule: P8, v6 → r1, Support: 12.58%, Confidence: 52.00%, Lift: 4.14, Conviction: 1.82
54. Rule: P8, v5 → r1, Support: 2.10%, Confidence: 50.00%, Lift: 23.54, Conviction: 1.96
55. Rule: P8, v5 → r0, Support: 2.10%, Confidence: 50.00%, Lift: 24.00, Conviction: 1.96
56. Rule: P5, v1 → r1, Support: 0.02%, Confidence: 50.00%, Lift: 2471.50, Conviction: 2.00
57. Rule: P5, v1 → r0, Support: 0.02%, Confidence: 50.00%, Lift: 2471.50, Conviction: 2.00
58. Rule: P1 → r0, Support: 1.51%, Confidence: 49.00%, Lift: 32.29, Conviction: 1.93
59. Rule: P8 → r0, Support: 13.67%, Confidence: 48.00%, Lift: 3.49, Conviction: 1.66
60. Rule: P7 → r1, Support: 2.79%, Confidence: 48.00%, Lift: 17.32, Conviction: 1.87
61. Rule: P1, v6 → r1, Support: 0.26%, Confidence: 46.00%, Lift: 174.91, Conviction: 1.85
62. Rule: P0, v2 → r1, Support: 0.12%, Confidence: 46.00%, Lift: 378.96, Conviction: 1.85
63. Rule: P5, v4 → r0, Support: 0.10%, Confidence: 45.00%, Lift: 444.87, Conviction: 1.82
64. Rule: P0, v4 → r1, Support: 0.08%, Confidence: 44.00%, Lift: 543.73, Conviction: 1.78
65. Rule: v5 → r1, Support: 4.92%, Confidence: 43.00%, Lift: 8.78, Conviction: 1.67
66. Rule: P5, v3 → r1, Support: 2.24%, Confidence: 43.00%, Lift: 19.15, Conviction: 1.71
67. Rule: P7, v3 → r1, Support: 0.49%, Confidence: 40.00%, Lift: 82.38, Conviction: 1.66
68. Rule: P6, v1 → r1, Support: 0.43%, Confidence: 40.00%, Lift: 94.15, Conviction: 1.66
69. Rule: P6, v4 → r0, Support: 0.04%, Confidence: 40.00%, Lift: 988.60, Conviction: 1.67
70. Rule: P2, v4 → r1, Support: 0.04%, Confidence: 40.00%, Lift: 988.60, Conviction: 1.67
71. Rule: P7, v5 → r0, Support: 0.50%, Confidence: 36.00%, Lift: 71.18, Conviction: 1.55
72. Rule: P4, v5 → r1, Support: 1.39%, Confidence: 35.00%, Lift: 25.07, Conviction: 1.52
73. Rule: P0 → r1, Support: 0.32%, Confidence: 33.00%, Lift: 101.95, Conviction: 1.49

74. Rule: P6, v3 → r1, Support: 0.63%, Confidence: 31.00%, Lift: 49.43, Conviction: 1.44

75. Rule: P6 → r1, Support: 3.16%, Confidence: 29.00%, Lift: 9.13, Conviction: 1.36

76. Rule: P4, v1 → r1, Support: 0.10%, Confidence: 29.00%, Lift: 286.69, Conviction: 1.41

77. Rule: P2, v6 → r1, Support: 0.04%, Confidence: 29.00%, Lift: 716.73, Conviction: 1.41

78. Rule: P3, v5 → r1, Support: 0.45%, Confidence: 27.00%, Lift: 60.66, Conviction: 1.36

79. Rule: P2, v3 → r1, Support: 0.59%, Confidence: 25.00%, Lift: 42.61, Conviction: 1.33

80. Rule: P8, v7 → r0, Support: 0.02%, Confidence: 25.00%, Lift: 1235.75, Conviction: 1.33

81. Rule: P1, v5 → r1, Support: 0.02%, Confidence: 25.00%, Lift: 1235.75, Conviction: 1.33

82. Rule: P3, v3 → r1, Support: 0.28%, Confidence: 24.00%, Lift: 84.74, Conviction: 1.31

83. Rule: P5, v2 → r1, Support: 0.10%, Confidence: 20.00%, Lift: 197.72, Conviction: 1.25

84. Rule: P5, v6 → r1, Support: 0.02%, Confidence: 20.00%, Lift: 988.60, Conviction: 1.25

85. Rule: P0, v0 → r1, Support: 0.02%, Confidence: 17.00%, Lift: 840.31, Conviction: 1.20

86. Rule: P4, v2 → r1, Support: 0.06%, Confidence: 9.00%, Lift: 148.29, Conviction: 1.10